

# Information Critical Phases under Decoherence

Akash Vijay<sup>1</sup> and Jong Yeon Lee<sup>1,2</sup>

<sup>1</sup>*Department of Physics and Anthony J. Leggett Institute of Condensed Matter Theory,  
University of Illinois at Urbana-Champaign, Urbana, Illinois 61801, USA*

<sup>2</sup>*Korea Institute for Advanced Study, Seoul 02455, South Korea*

(Dated: December 29, 2025)

Quantum critical phases are extended regions of phase space characterized by a diverging correlation length. By analogy, we define an *information critical phase* as an extended region of a mixed state phase diagram where the Markov length, the characteristic length scale governing the decay of the conditional mutual information (CMI), diverges.

We demonstrate that such a phase arises in decohered  $\mathbb{Z}_N$  Toric codes by assessing both the CMI and the coherent information, the latter quantifying the robustness of the encoded logical qudits. For  $N > 4$ , we find that the system hosts an information critical phase intervening between the decodable and non-decodable phases where the coherent information saturates to a fractional value in the thermodynamic limit, indicating that a finite fraction of logical information is still preserved. We show that the density matrix in this phase can be decomposed into a convex sum of Coulombic pure states, where gapped anyons reorganize into gapless photons. We further consider the ungauged  $\mathbb{Z}_N$  Toric code and interpret its mixed state phase diagram in the language of strong-to-weak spontaneous symmetry breaking. We argue that in the dual model, the information critical phase arises because the spontaneously broken off-diagonal  $\mathbb{Z}_N$  symmetry gets enhanced to a U(1) symmetry, resulting in a novel superfluid phase whose gapless modes involve coherent excitations of both the system and the environment. Finally, we propose an optimal decoding protocol for the corrupted  $\mathbb{Z}_N$  Toric code and evaluate its effectiveness in recovering the fractional logical information preserved in the information critical phase. Our findings identify a gapless analog for mixed-state phases that still acts as a fractional topological quantum memory, thereby extending the conventional paradigm of quantum memory phases.

## CONTENTS

I. Introduction	1	A. Diagonalization of decohered density matrices	20
II. Preliminaries	3	1. Diagonalization of $\mathcal{E}(\rho_Q)$	20
A. $\mathbb{Z}_N$ Toric code	3	2. Diagonalization of $\mathcal{E}(\rho_{QR})$	21
B. Qudit decoherence channels	5		
C. Information Diagnostics	5		
D. Analytic Diagonalization	6	B. Deriving Eq. (35) for the Conditional Mutual	22
1. Coherent Information	7	Information	
2. Conditional Mutual Information	7	C. Relative Entropy	23
E. Random Bond Clock Models	7	D. Random Bond Clock Models	23
III. Information Critical Phases	9	1. Coherent Information	23
A. Intrinsic mixed-state behavior	9	a. Low Temp Limit	24
B. Numerical details	10	b. High Temp Phase	24
C. $N \leq 4$	10	c. QLRO Phase	24
D. $N > 4$	11	2. CMI	25
E. Critical points and self-duality	11		
IV. Separability Transitions	12		
V. Dual Strong-to-Weak SSB	13		
VI. Decoding Protocols	15		
VII. Discussion	16		
Acknowledgments	17	I. INTRODUCTION	
References	17	Quantum information is inherently fragile in the presence of environmental noise. Thus, the formulation and design of robust quantum error-correcting codes is an indispensable aspect of any viable theory of quantum computation [1–5]. In particular, topological codes offer a promising route to realize fault-tolerant quantum memories and scalable quantum processors [6–14]. They also provide a physical realization of novel phases of matter with ground state degeneracy and long range entanglement [15–20]. Considerable effort has gone into determining the error thresholds of topological quantum codes [21–25]. Early studies operationally defined these	

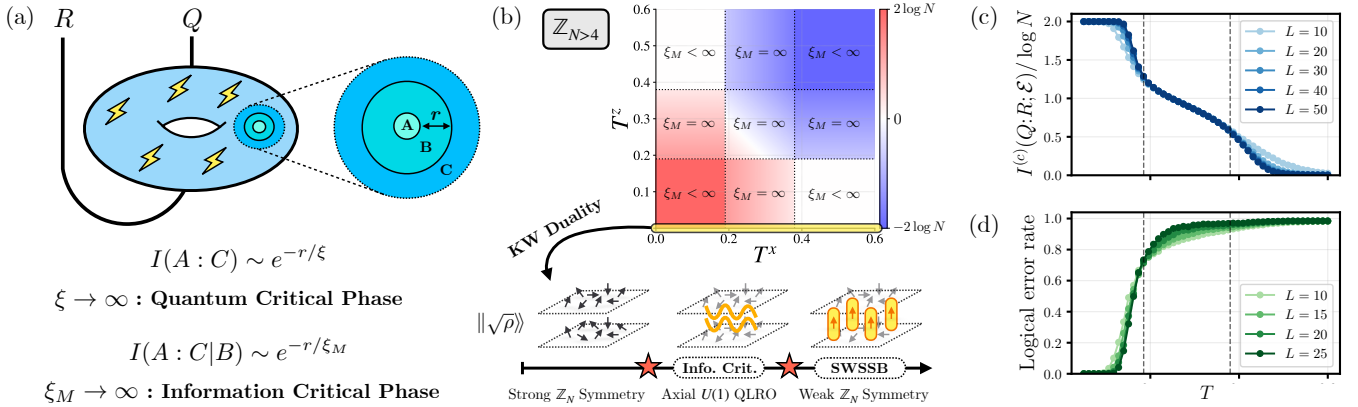


FIG. 1. (a) **Information critical phase.** The Markov length  $\xi_M$  sets the length scale for the spatial decay of the conditional mutual information  $I(A:C|B)$ , analogous to how the correlation length  $\xi$  controls the decay of the mutual information. An *information critical phase* is an extended region where  $\xi_M = \infty$ . (b) **Phase Diagram.** We map the mixed-state phase diagram of the  $\mathbb{Z}_{N>4}$  toric code as a function of effective temperatures  $T^x$  and  $T^z$ , which parametrize the strengths of  $X$ - and  $Z$ -dephasing, respectively. Throughout the diagram  $\xi = 0$  while the Markov length can diverge. The ungauged description admits a strong-to-weak SSB interpretation. The dual spin model evolves from a strongly  $\mathbb{Z}_N$ -symmetric phase into an intermediate regime where the broken axial  $\mathbb{Z}_N$  symmetry effectively enhances to an emergent  $U(1)$  symmetry, giving rise to a quasi-long range ordered superfluid phase. Further increasing the decoherence strength eventually causes full SWSSB of the  $\mathbb{Z}_N$  symmetry. (c) **Coherent information.** For  $N = 8$ , we plot the normalized  $I^{(c)}$  as a function of  $T$  across different system sizes. It approaches its maximal value for  $T < 0.185$ , and remains finite in the information-critical regime  $0.185 < T < 0.38$ , indicating *fractionally recoverable* logical information. For  $T > 0.38$ , it decays to zero. (d) **Logical error rate.** We devise an optimal decoder that combines a minimum-integer-cost-flow solver with a subsequent worm-algorithm refinement. The decoder has a threshold that coincides with the point at which the Toric code exits the perfectly decodable phase. Within the fractionally decodable phase, we find that the decoder is unsuccessful, indicating the need for a different type of decoder.

thresholds by assessing the success or failure of specific decoding protocols. More recent work reframes the decodability transition as an intrinsic mixed-state phase transition, in which information-theoretic quantities exhibit a sharp, non-analytic jump [26–33]. This reflects a fundamental change in the mixed state order of the system, that is independent of any specific decoder.

For pure states, two states are said to be in the same phase if their parent Hamiltonians can be adiabatically connected along a continuous, finite path in parameter space without encountering a divergent correlation length. This is equivalent to the existence of a finite-depth (quasi)-local unitary (FDLU) circuit that maps one state to the other [34–37]. For mixed states, the absence of a similar notion of a parent Hamiltonian renders an analogous classification scheme far less straightforward. Nevertheless, in recent years, there have been various attempts to provide a comprehensive classification of such phases [38–58], and one of the key objects that has emerged in this discussion is the *Markov length*. It is the characteristic length scale governing the decay of the conditional mutual information (CMI), just as the correlation length is the characteristic length scale governing the decay of the mutual information (MI) (see Fig. 1). The operational significance of the Markov length stems from the fact that any finite depth local quantum channel that preserves the finiteness of the Markov length is (quasi)-locally reversible [48, 56]. Thus, the Markov length is the natural analog of the correlation length for

classifying mixed-state phases; it is expected to be finite within each phase and diverge only at criticality.

In pure-state criticality, both the correlation length and the Markov length diverge together. However, in mixed states, these two length scales need not track each other, opening up a new possibility: a phase with a diverging Markov length but a finite correlation length. In this work, we broaden the landscape of mixed-state phases by introducing the notion of an *information critical phase*, defined as an extended region of a mixed-state phase diagram with precisely this separation of scales.

As a prototypical example, we examine two-dimensional  $\mathbb{Z}_N$  Toric codes subject to  $X$  and  $Z$  decoherence channels. Unlike the  $\mathbb{Z}_2$  toric code, which exhibits a single transition from a decodable long-range-entangled phase to a non-decodable short-range-entangled phase, we find that for  $N > 4$ , the  $\mathbb{Z}_N$  toric code can host three distinct phases. In addition to the familiar decodable and non-decodable phases, we obtain an information critical phase in which the Markov length diverges throughout while the correlation length remains finite.

First, we use analytic diagonalization techniques [27, 28, 30] to express both the CMI and the coherent information in terms of partition functions of two dimensional disordered  $\mathbb{Z}_N$  clock models along the Nishimori line. Within this mapping, the information critical phase is identified with the quasi-long-range-ordered (QLRO) phase of the disordered clock model. The QLRO phase intervenes between the ordered and disordered

phases and is known to exist along the Nishimori line for  $N > 4$  [59–64]. The divergence of the Markov length then follows directly from the divergence of the correlation length in the corresponding clock model. In Sec. III, we find that the coherent information in the information critical phase saturates to a fractional value in the thermodynamic limit, interpolating between its values in the decodable and non-decodable phases and decreasing continuously with increasing decoherence strength (see Fig. 1). This behavior reveals the persistence of *fractional recoverable logical information* in this phase.

In Sec. IV, using the “minimally entangled typical thermal state” ansatz [41, 53, 65], we show that the decohered density matrix in the information critical phase can be expressed as a convex ensemble of pure states which exhibit power law correlations for string operators. These pure states belong to a Coulomb phase, where gapped anyons reorganize into gapless photons.

In Sec. V, we also consider the mixed state phase diagram of the “ungaught”  $\mathbb{Z}_N$  Toric code obtained via Kramers-Wannier (KW) duality. Under the duality, the phase diagram can be a naturally understood in the language of strong-to-weak spontaneous symmetry breaking (SWSSB) [27, 66–73]. In the KW dual model, increasing the decoherence strength causes the strong  $\mathbb{Z}_N$  symmetry to spontaneously break to a weak  $\mathbb{Z}_N$  symmetry. For  $N > 4$ , an intermediate information critical phase emerges where the broken off-diagonal  $\mathbb{Z}_N$  symmetry is effectively enhanced to a continuous  $U(1)$  symmetry, giving rise to new gapless modes involving collective excitations of both the system and the environment. This yields a novel *superfluid* phase in these decohered discrete spin systems. We emphasize that the  $\mathbb{Z}_N$  symmetry is inherited from  $\mathbb{Z}_N$  anyon charge conservation in the original topological model. Although the net anyon charge remains fixed (in particular, zero) even in the presence of decoherence, sufficiently strong noise can proliferate anyon pairs, triggering a SWSSB.

Finally, in Sec. VI, we consider the problem of decoding the noise corrupted  $\mathbb{Z}_N$  Toric code [21, 74–79]. We propose an optimal decoding protocol for the  $\mathbb{Z}_N$  Toric code that combines a *minimum integer cost flow solver* with a worm algorithm refinement. We demonstrate that this decoder exhibits a threshold that coincides precisely with the point at which the Toric code exits the decodable phase. We conclude by assessing the decoder’s ability to recover the fractional logical information that remains protected within the information critical phase.

Our results uncover a new gapless analog of mixed state phases that still functions as a fractional topological memory, thereby extending the landscape of quantum memory phases beyond the conventional gapped paradigm.

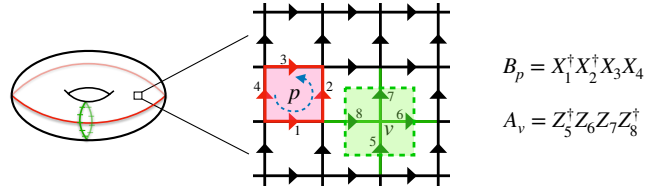


FIG. 2. The plaquette and vertex stabilizers of the  $\mathbb{Z}_N$  Toric code.

## II. PRELIMINARIES

In this section, we review several key concepts required for the main analysis. Readers familiar with this material may skip the corresponding subsections. In Sec. II A, we define the  $\mathbb{Z}_N$  generalization of the Toric code and define the anyon basis that will be used for the subsequent exact diagonalization. In Sec. II B, we discuss the generalization of independent Pauli  $X$  and  $Z$  errors on qudits, emphasizing the symmetries of the channel. In Sec. II C, we review the information-theoretic quantities that will serve as our primary diagnostics throughout the paper. In Sec. II D, we perform analytic diagonalization and express information-theoretic quantities in terms of partition functions of the disordered statistical mechanics model. In Sec. II E, we provide a review on random bond clock models.

### A. $\mathbb{Z}_N$ Toric code

A  $\mathbb{Z}_N$  generalization of the Toric code is obtained by placing  $N$ -dimensional qudits on the edges of an  $L \times L$  square lattice with periodic boundary conditions in both the  $\hat{x}$  and  $\hat{y}$  directions. Each qudit Hilbert space hosts a  $\mathbb{Z}_N$  Pauli algebra which is generated by unitary operators  $X$  and  $Z$ , obeying  $X^N = Z^N = 1$  and  $ZX = \omega XZ$ , where  $\omega = e^{2\pi i/N}$  is the fundamental  $N$ th root of unity.

We equip each link  $\mu$  with an orientation as in Fig. 2: horizontal links are along  $\hat{x}$ , and vertical links are along  $\hat{y}$ . The stabilizer operators of the code are geometrically local and come in two kinds: Plaquette stabilizers  $B_p$  and vertex stabilizers  $A_v$ :

$$A_v = \prod_{\text{tail}(\mu)=v} Z_\mu \prod_{\text{head}(\mu)=v} Z_\mu^\dagger \quad (1)$$

$$B_p = \prod_{\substack{\mu \in \partial p \\ \circlearrowleft}} X_\mu \prod_{\substack{\mu \in \partial p \\ \circlearrowright}} X_\mu^\dagger \quad (2)$$

Note that by convention, we choose each plaquette  $p$  to be counter-clockwise oriented. It is easy to verify that all these stabilizer operators commute with one another.

The logical space is defined by the condition:  $A_v |\psi\rangle = B_p |\psi\rangle = |\psi\rangle$  for all vertices  $v$  and all plaquettes  $p$ . Equiv-

alently, it is the ground state subspace of the

$$H = - \sum_v \left( \frac{A_v + A_v^\dagger}{2} \right) - \sum_p \left( \frac{B_p + B_p^\dagger}{2} \right). \quad (3)$$

$A_v = 1$  is the Gauss Law constraint (no electric charges) whereas the  $B_p = 1$  imposes local flatness of the gauge field (no magnetic fluxes). Although we have  $L^2$  vertex stabilizers and  $L^2$  plaquette stabilizers, they obey the global constraints  $\prod_v A_v = \prod_p B_p = 1$  owing to the fact that the above products always involve both  $X_\mu$  ( $Z_\mu$ ) and  $X_\mu^\dagger$  ( $Z_\mu^\dagger$ ) for each link  $\mu$ . Thus the number of independent stabilizer constraints is really  $2L^2 - 2$  which means that the logical subspace consists of  $2L^2 - (2L^2 - 2) = 2$  independent qudits. These can be acted on via logical operators, i.e., non-contractible Wilson and 't Hooft loops which wind around the two cycles of the torus.

The Wilson strings live on the direct lattice and involve products of Pauli  $X$  operators. For an oriented direct lattice curve  $\gamma$ , the Wilson string which creates electric charges  $\pm k$  (violations of the vertex stabilizer condition as  $A_v = e^{\pm 2\pi i k/N}$ ) on the two ends of  $\gamma$  is given by

$$X_\gamma^k = \prod_{\mu \in \gamma} X_\mu^k \quad (4)$$

Note that if  $\mu$  is oriented in the same sense as  $\gamma$ , we multiply by  $X_\mu^k$  and if it's oriented in the opposite sense as  $\gamma$ , we multiply by  $(X_\mu^k)^\dagger$ .

The 't Hooft strings, on the other hand, live on the dual lattice and involve products of Pauli  $Z$  operators of links which transversely cut the dual loop. For an oriented dual lattice curve  $\hat{\gamma}$ , the 't Hooft string which creates magnetic fluxes  $\pm k$  (violations of the plaquette stabilizer condition as  $B_p = e^{\pm 2\pi i k/N}$ ) on the 2 ends of  $\hat{\gamma}$  is given by

$$Z_\gamma^k = \prod_{\mu \perp \hat{\gamma}} Z_\mu^k \quad (5)$$

We adopt the convention that if  $\mu$  cuts  $\hat{\gamma}$  from left to right, we multiply by  $Z_\mu^k$  and if it cuts from right to left, we multiply by  $(Z_\mu^k)^\dagger$ . Wilson strings are often referred to as *electric strings* whereas 't Hooft strings are commonly referred to as *magnetic strings*. Closed Wilson and 't Hooft loops do not create any charges or fluxes and leave the logical space invariant. In fact, *contractible* Wilson and 't Hooft loops are written as products of stabilizers, thus acting as the identity on the logical space.

On the other hand, *non-contractible* Wilson and 't Hooft loops act nontrivially on the logical space. Consider two non-contractible direct lattice loops  $\mathcal{C}_1$  and  $\mathcal{C}_2$  which wind around the two cycles of the torus. We can associate a charge-1 Wilson loop to each of these cycles, denoted  $X_{\hat{\mathcal{C}}_1}$  and  $X_{\mathcal{C}_2}$  respectively. Similarly consider two non-contractible dual lattice loops  $\hat{\mathcal{C}}_1$  and  $\hat{\mathcal{C}}_2$  which also wind around the two cycles of the torus. We can associate a flux-1 't Hooft loop to each of these cycles, denoted  $Z_{\hat{\mathcal{C}}_1}$

and  $Z_{\hat{\mathcal{C}}_2}$  respectively. The operators  $\{X_{\hat{\mathcal{C}}_1}, Z_{\hat{\mathcal{C}}_2}, X_{\mathcal{C}_2}, Z_{\mathcal{C}_1}\}$  obey the  $\mathbb{Z}_N$  Pauli algebra and so they represent the Pauli  $X$  and  $Z$  operators for the 2 logical qudits.

**Logical states.** Any logical state is a superposition of all closed, contractible (electric) string-net states. In particular, the logical state  $|\Psi_0\rangle$  with logical eigenvalues  $(Z_{\hat{\mathcal{C}}_1}, Z_{\hat{\mathcal{C}}_2}) = (1, 1)$  can be written it as

$$|\Psi_0\rangle = \frac{1}{N^{L^2}} \sum_{\theta_p \in \mathbb{Z}_N} \prod_p B_p^{\theta_p} |\{Z_\mu = +1\}\rangle \quad (6)$$

since  $B_p^{\theta_p}$  creates a closed loop of strength  $\theta_p$  around plaquette  $p$ . By acting with the logical operators  $X_{\mathcal{C}_1}^{a_1}$  and  $X_{\mathcal{C}_2}^{a_2}$  with  $a_1, a_2 \in \mathbb{Z}_N$ , we can create electric loops of different charge winding around the non-contractible cycles of the torus. Therefore, a pair  $\mathbf{a} := (a_1, a_2)$  labels a set of orthonormal bases for the entire logical space.

**Anyon basis.** The eigenstates of the stabilizer Hamiltonian in Eq. (3) can be completely labeled by sets of eigenvalues  $\mathbf{e} = \{e_v\}$ ,  $\mathbf{m} = \{m_p\}$ , and  $\mathbf{a}$  of  $\{A_v\}$ ,  $\{B_p\}$ ,  $\{Z_{\hat{\mathcal{C}}_i}\}$ , respectively. Denoting it as  $|\mathbf{e}; \mathbf{m}; \mathbf{a}\rangle$ , it labels local and global anyon excitations with respect to  $|\Psi_0\rangle$ .

Starting from  $|\Psi_0\rangle$  in Eq. (6), we can construct the state  $|\mathbf{e}; \mathbf{m}; \mathbf{a}\rangle$  by acting with some set of Wilson and 't Hooft strings. For this, we choose the Wilson and 't Hooft strings that create anyons  $e_v$  and  $m_p$  at their endpoints, respectively. Similarly, we choose the Wilson loops that create non-contractible electric strings which wind around the 2 cycles of the torus in accordance with the logical eigenvalues  $\mathbf{a}$ . Let  $\mathbf{k}^{e/m}$  be a set of  $\mathbb{Z}_N$  values on links. Then we can write

$$|\mathbf{e}; \mathbf{m}; \mathbf{a}\rangle = Z^{\mathbf{k}^m} X^{\mathbf{k}^e} |\Psi_0\rangle \quad (7)$$

where  $X^{\mathbf{k}^e} = \prod_\mu X_\mu^{k_\mu^e}$  and  $Z^{\mathbf{k}^m} = \prod_\mu Z_\mu^{k_\mu^m}$  collectively denotes the product of Wilson and 't Hooft string operators, respectively.  $(\mathbf{e}; \mathbf{m})$  and  $\mathbf{ks}$  are related by

$$\begin{aligned} (\nabla \cdot \mathbf{k}^e)_v &\equiv \sum_{\mu: \text{tail}(\mu)=v} \mathbf{k}_\mu^e - \sum_{\mu: \text{head}(\mu)=v} \mathbf{k}_\mu^e = e_v \mod N \\ (\nabla \times \mathbf{k}^m)_p &\equiv \sum_{\substack{\mu \in \partial p \\ \textcircled{O}}} \mathbf{k}_\mu^m - \sum_{\substack{\mu \in \partial p \\ \textcircled{O}}} \mathbf{k}_\mu^m = m_p \mod N \end{aligned} \quad (8)$$

If we view  $\mathbf{k}^e$  and  $\mathbf{k}^m$  as  $\mathbb{Z}_N$  valued flows, then the charges ( $e_v$ ) act as sources in  $\mathbf{k}^e$  whereas the fluxes ( $m_p$ ) act as vortices in  $\mathbf{k}^m$ . We also introduce the following succinct notation to denote the eigenvalues of states  $X^{\mathbf{k}^e} |\Psi_0\rangle$  with respect to non-contractible 't Hooft loops on the dual lattice ( $\hat{\mathcal{C}}$ ) and the eigenvalues of states  $Z^{\mathbf{k}^m} |\Psi_0\rangle$  with respect to non-contractible Wilson loops on the direct lattice ( $\mathcal{C}$ ).

$$\hat{\mathcal{C}}(\mathbf{k}^e) = \mathbf{a} \iff Z_{\hat{\mathcal{C}}_{2(1)}}[X^{\mathbf{k}^e} |\Psi_0\rangle] = \omega^{a_{1(2)}} X^{\mathbf{k}^e} |\Psi_0\rangle \quad (9)$$

Thus,  $Z^{\mathbf{k}^m} X^{\mathbf{k}^e} |\Psi_0\rangle = |\mathbf{e}; \mathbf{m}; \mathbf{a}\rangle$  iff  $\mathbf{k}^e$  and  $\mathbf{k}^m$  satisfy the conditions in Eq. (8) and additionally  $\hat{\mathcal{C}}(\mathbf{k}^e) = \mathbf{a}$ .

## B. Qudit decoherence channels

For qudits, a generic  $X$  or  $Z$  type dephasing channel takes the form

$$\mathcal{E}^x(\rho) = \sum_{k=0}^{N-1} p_k^x X^k \rho (X^\dagger)^k, \quad (10)$$

$$\mathcal{E}^z(\rho) = \sum_{k=0}^{N-1} p_k^z Z^k \rho (Z^\dagger)^k. \quad (11)$$

Each channel is specified by  $N - 1$  independent real parameters  $p_k^{x,z} \geq 0$ , subject to the normalization constraint  $\sum_{k=0}^{N-1} p_k^{x,z} = 1$ . In the rest of the paper, we only consider dephasing channels which preserve *charge conjugation symmetry*:  $p_k^{x,z} = p_{N-k}^{x,z}$ . In the following sections, we show that the spectrum of the decohered density matrix can be mapped onto the partition function of a two-dimensional disordered spin model, with symmetries determined by the parameters  $p_k^{x,z}$ . For our purposes, only the long-distance behavior is relevant, and thus the phase structure is governed solely by the symmetry class of the associated statistical-mechanics model rather than by the specific microscopic values of these parameters. In particular, for charge-conjugation-symmetric dephasing channels, the relevant symmetry group is the dihedral group  $D_N = \mathbb{Z}_N \rtimes \mathbb{Z}_2^P$ , and the corresponding models are found to be non-chiral clock models. Different choices of  $p_k^{x,z}$  can shift non-universal details, but they do not change the qualitative phase diagram.

## C. Information Diagnostics

In this section, we introduce the key information measures that will play a central role in the rest of the paper. Throughout this section, we shall view the  $\mathbb{Z}_N$  Toric code system,  $Q$ , as a quantum memory that encodes two qudits worth of information in its logical space. The code is then subject to a noisy channel  $\mathcal{E}$  which factorizes over physical links  $\mathcal{E} = \bigotimes_\mu \mathcal{E}_\mu$ . We focus on measures that quantify the robustness of the encoded logical information and probe the local structure of correlations.

**Coherent Information.** Coherent information is the currency of quantum error correction. It upper bounds the amount of quantum information that can ultimately be recovered following the application of the noisy channel [80–84]. To mathematically define it, we first introduce a reference system  $R$  consisting of 2 qudits which are maximally entangled with the 2 logical qudits of the  $\mathbb{Z}_N$  Toric code  $Q$ . Together they are in the Bell state

$$|\Psi\rangle_{QR} = \frac{1}{\sqrt{N^2}} \sum_{\mathbf{a}} X^{\mathbf{a}} |\Psi_0\rangle_Q \otimes |\mathbf{a}\rangle_R \quad (12)$$

Here  $X^{\mathbf{a}} \equiv X_{C_1}^{a_1} X_{C_2}^{a_2}$  and  $|\mathbf{a}\rangle_R = |a_1, a_2\rangle_R$  with  $a_i = 0, \dots, N - 1$ . The density matrix of the composite  $QR$

system is  $\rho_{QR} = |\Psi\rangle_{QR}\langle\Psi|_{QR}$  whereas the reduced density matrix of  $Q$  is found to be a classical mixture of all logical states

$$\rho_Q = \frac{1}{N^2} \sum_{\mathbf{a}} X^{\mathbf{a}} |\Psi_0\rangle_Q \langle\Psi_0|_Q (X^{\mathbf{a}})^\dagger \quad (13)$$

The coherent information between the reference qudits  $R$  and the Toric code  $Q$  following the application of a quantum channel  $\mathcal{E}$ , which acts solely on  $Q$ , is given by

$$I^{(c)}(Q : R; \mathcal{E}) = S(\mathcal{E}(\rho_Q)) - S(\mathcal{E}(\rho_{QR})) \quad (14)$$

$I^{(c)}(Q : R; \mathcal{E})$  bounds the amount of information that can be retrieved from the state  $\mathcal{E}(\rho_Q)$ . Since the coherent information obeys the data processing inequality,  $I^{(c)}(Q : R; \mathcal{E}_1 \circ \mathcal{E}_2) \leq I^{(c)}(Q : R; \mathcal{E}_2)$ , the amount of information that is lost as a consequence of noise can never be recovered by post-processing. It is for this reason that  $I^{(c)}(Q : R; \mathcal{E})$  gives an algorithm independent upper bound on recoverable information. As a consequence of the sub-additivity of entropy, it is easy to see that

$$-2 \log N \leq I^{(c)}(Q : R; \mathcal{E}) \leq 2 \log N \quad (15)$$

A positive coherent information heralds distillable entanglement whereas a negative coherent information points to consumption of entanglement by the noisy channel. A negative coherent information does not by itself preclude the retrievability of classical information encoded in the state.

**Conditional Mutual Information.** Let  $A$  denote a spatial subregion and let  $\rho_A = \text{Tr}_{\overline{A}} \rho$  be its reduced density matrix. The Von-Neumann entanglement entropy is given by

$$S(A) = -\text{tr} \rho_A \log \rho_A \quad (16)$$

For a tripartite state  $\rho_{ABC}$ , the quantum conditional mutual information (CMI) is given by

$$I(A : C | B) = S(AB) + S(BC) - S(B) - S(ABC) \quad (17)$$

It quantifies the residual correlations (classical + quantum) between  $A$  and  $C$  that remain when the buffer region  $B$  is known. By strong subadditivity, the CMI is non-negative and obeys the data-processing inequality. Moreover,  $I(A : C | B) = 0$  iff  $\rho_{ABC}$  forms a quantum Markov state, namely  $\rho_{ABC}$  admits a direct-sum decomposition of the form

$$\rho_{ABC} = \bigoplus_i \rho_{AB_i^L} \otimes \rho_{B_i^R C} \quad (18)$$

where the Hilbert space of subregion  $B$  also decomposes as  $\mathcal{H}_B = \bigoplus_i \mathcal{H}_{B_i^L} \otimes \mathcal{H}_{B_i^R}$ . In this case, the tripartite state  $\rho_{ABC}$  can be exactly recovered from marginals  $\rho_{AB}$  or  $\rho_{BC}$  via the Petz recovery map [85]. More generally, if  $I(A : C | B) \leq \epsilon$  for some small, nonzero  $\epsilon$ , there exist recovery channels  $\mathcal{R}_{B \rightarrow BC}$  (and  $\mathcal{R}_{B \rightarrow AB}$ ) (such as the

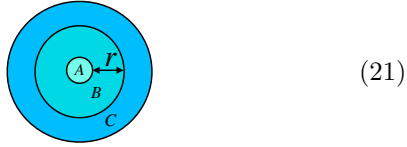
twirled-Petz maps) such that the reconstructed states  $\mathcal{R}_{B \rightarrow BC}(\rho_{AB})$  and  $\mathcal{R}_{B \rightarrow AB}(\rho_{BC})$  approach  $\rho_{ABC}$  with high fidelity [86].

$$F(\rho_{ABC}, \mathcal{R}_{B \rightarrow BC}(\rho_{AB})) \geq 2^{-\epsilon/2} \quad (19)$$

$$F(\rho_{ABC}, \mathcal{R}_{B \rightarrow AB}(\rho_{BC})) \geq 2^{-\epsilon/2} \quad (20)$$

In this sense, the CMI quantifies approximate recoverability of  $\rho_{ABC}$  from the marginals  $\rho_{AB}$  or  $\rho_{BC}$ .

We shall be interested in CMI for the following geometric partition



In non-critical models, the CMI for this geometry is expected to decay exponentially with the width of  $B$ :

$$I(A : C|B) \sim \text{poly}(|A|, |C|)e^{-r/\xi_M} \quad (22)$$

where  $\xi_M$  is the *Markov Length* [48, 56, 57]. If  $\xi_M$  is finite, a small buffer region  $B$  is sufficient to render  $I(A : C|B) \approx 0$  implying conditional independence and approximate recoverability of the tripartite state  $\rho_{ABC}$  from its marginal  $\rho_{AB}$ . By contrast, if  $\xi_M = \infty$ , achieving approximate recoverability requires a buffer region  $B$  whose width scales with the size of  $A$ , reflecting the presence of long range correlations.

The Markov length can be viewed as a *conditional correlation length* as it quantifies the spatial locality of correlations between  $A$  and  $C$  upon conditioning on the buffer region  $B$ . Crucially, if  $\xi_M$  remains finite along a path of evolution generated by a local Lindbladian, then one can construct a quasi-local quantum channel that approximately inverts the evolution, implying that all intermediate states remain in the same mixed state phase [48]. This is the main operational significance of the Markov length, and in this sense it plays the same role in classifying mixed state phases that the ordinary correlation length plays in classifying pure state phases. If the Markov length diverges, we encounter a mixed-state critical point.

#### D. Analytic Diagonalization

Next, we analytically diagonalize the decohered density matrix of the  $\mathbb{Z}_N$  Toric code in order to compute the information-theoretic quantities introduced above. Let  $\rho_Q$  denote the initial reduced density matrix of the Toric code, as defined in Eq. (13). We subject each physical qudit to independent  $X$  and  $Z$  dephasing channels, specified in Eq. (10), with channel parameters  $\{p_k^{x,z}\}$  taken

to be identical across all qudits. The resulting post-decoherence density matrix is

$$\mathcal{E}(\rho_Q) = \left( \prod_{\mu} \mathcal{E}_{\mu}^x \circ \prod_{\mu} \mathcal{E}_{\mu}^z \right) (\rho_Q) \quad (23)$$

where  $\mu$  labels the links of the lattice. An important feature of the above channel is that  $\mathcal{E}(\rho_Q)$  commutes with all the stabilizer operators  $A_v$  and  $B_p$ :

$$A_v \mathcal{E}_{\mu}^{x,z}(\rho_Q) = \mathcal{E}_{\mu}^{x,z}(\rho_Q) A_v \quad (24)$$

$$B_p \mathcal{E}_{\mu}^{x,z}(\rho_Q) = \mathcal{E}_{\mu}^{x,z}(\rho_Q) B_p \quad (25)$$

Thus  $\mathcal{E}(\rho_Q)$  can be simultaneously diagonalize with the full stabilizer algebra. Note however that  $\mathcal{E}_{\mu}^z(\rho_Q)$  and  $\mathcal{E}_{\mu}^x(\rho_Q)$  needn't actually commute with the logical operators  $X_{C_1}^{a_1}$  and  $X_{C_2}^{a_2}$ . In Appendix A, we show that  $\mathcal{E}(\rho_Q)$  can be expanded as follows

$$\mathcal{E}(\rho_Q) = \sum_{\substack{\mathbf{e}; \mathbf{m} \\ \mathbf{a}}} \frac{1}{N^2} \mathcal{Z}[\mathbf{e}] \mathcal{Z}[\mathbf{m}] |\mathbf{e}; \mathbf{m}; \mathbf{a}\rangle \langle \mathbf{e}; \mathbf{m}; \mathbf{b}| \quad (26)$$

where  $\mathcal{Z}[\mathbf{e}, \mathbf{a}]$  and  $\mathcal{Z}[\mathbf{m}, \mathbf{b}]$  are defined as

$$\mathcal{Z}[\mathbf{e}, \mathbf{a}] = \sum_{\substack{(\nabla \times \mathbf{k}^x)_v = e_v \\ \hat{C}(\mathbf{k}^x) = \mathbf{a}}} \prod_{\mu} p_{k_{\mu}^x}^x \quad (27)$$

$$\mathcal{Z}[\mathbf{m}, \mathbf{b}] = \sum_{\substack{(\nabla \times \mathbf{k}^z)_p = m_p \\ \hat{C}(\mathbf{k}^z) = \mathbf{b}}} \prod_{\mu} p_{k_{\mu}^z}^z \quad (28)$$

and furthermore  $\mathcal{Z}[\mathbf{e}] = \sum_{\mathbf{a}} \mathcal{Z}[\mathbf{e}, \mathbf{a}]$  and  $\mathcal{Z}[\mathbf{m}] = \sum_{\mathbf{b}} \mathcal{Z}[\mathbf{m}, \mathbf{b}]$ . Note that due to the normalization of  $\{p_k^{x,z}\}$ , we have  $\sum_{\mathbf{e}, \mathbf{a}} \mathcal{Z}[\mathbf{e}, \mathbf{a}] = \sum_{\mathbf{m}, \mathbf{b}} \mathcal{Z}[\mathbf{m}, \mathbf{b}] = 1$ . In the next section, we show that these are normalized partition functions of two-dimensional disordered classical spin models. More precisely,  $\mathcal{Z}[\mathbf{e}, \mathbf{a}]$  ( $\mathcal{Z}[\mathbf{m}, \mathbf{a}]$ ) is the current loop representation of a disordered  $\mathbb{Z}_N$  clock model on the direct (dual) lattice, evaluated within a fixed homology sector. The charges ( $\mathbf{e}$ ) and fluxes ( $\mathbf{m}$ ) play the role of frustrations in these disordered models.

Similarly in order to diagonalize  $\mathcal{E}(\rho_{QR})$ , it is convenient to introduce a new orthonormal basis of the Toric code + reference Hilbert space which is defined as follows

$$|\mathbf{e}; \mathbf{m}; \mathbf{a}, \mathbf{b}\rangle_{QR} = \sum_{\mathbf{c}} \omega^{\mathbf{b} \cdot \mathbf{c}} |\mathbf{e}; \mathbf{m}; \mathbf{a} + \mathbf{c}\rangle_Q \otimes |\mathbf{c}\rangle_R$$

We show in Appendix A that  $\mathcal{E}(\rho_{QR})$  is now fully diagonal in this new basis and is given by

$$\mathcal{E}(\rho_{QR}) = \sum_{\mathbf{a}, \mathbf{b}} \sum_{\mathbf{e}; \mathbf{m}} \mathcal{Z}[\mathbf{e}, \mathbf{a}] \mathcal{Z}[\mathbf{m}, \mathbf{b}] |\mathbf{e}; \mathbf{m}; \mathbf{a}, \mathbf{b}\rangle_{QR} \langle \mathbf{e}; \mathbf{m}; \mathbf{a}, \mathbf{b}|_{QR} \quad (29)$$

Once again, we find that the spectrum of the density matrix is precisely determined by the partition functions  $\mathcal{Z}[\mathbf{e}, \mathbf{a}]$  and  $\mathcal{Z}[\mathbf{m}, \mathbf{b}]$ . Note that the effect of  $X$  and  $Z$  decoherence decouples in the final expression in both  $\mathcal{E}(\rho_Q)$  and  $\mathcal{E}(\rho_{QR})$ .

### 1. Coherent Information

We now derive exact expressions for the information measures introduced in section (II C) and express them in terms of  $\mathcal{Z}[\mathbf{e}, \mathbf{a}]$  and  $\mathcal{Z}[\mathbf{m}, \mathbf{b}]$ . Our analysis bypasses using Renyi proxies and instead focuses directly on quantities carrying direct operational meaning. This is useful since we do not rely on any analytic continuation.

The coherent information is a difference of two Von-Neumann entropies:

$$I^{(c)}(Q : R; \mathcal{E}) = S(\mathcal{E}(\rho_Q)) - S(\mathcal{E}(\rho_{QR})) \quad (30)$$

Since we've diagonalised both  $\mathcal{E}(\rho_Q)$  and  $\mathcal{E}(\rho_{QR})$ , we can write down a simple, exact closed form expression for  $I^{(c)}(Q : R; \mathcal{E})$ . First note that the Von-Neumann entropy of  $\mathcal{E}(\rho_Q)$  is

$$\begin{aligned} S(\mathcal{E}(\rho_Q)) &= 2 \log N - \sum_{\mathbf{e}} \mathcal{Z}[\mathbf{e}] \log \mathcal{Z}[\mathbf{e}] \\ &\quad - \sum_{\mathbf{m}} \mathcal{Z}[\mathbf{m}] \log \mathcal{Z}[\mathbf{m}] \end{aligned} \quad (31)$$

On the other hand the Von-Neumann entropy of  $\mathcal{E}(\rho_{QR})$  is given by

$$\begin{aligned} S(\mathcal{E}(\rho_{QR})) &= - \sum_{\mathbf{e}, \mathbf{a}} \mathcal{Z}[\mathbf{e}, \mathbf{a}] \log \mathcal{Z}[\mathbf{e}, \mathbf{a}] \\ &\quad - \sum_{\mathbf{m}, \mathbf{b}} \mathcal{Z}[\mathbf{m}, \mathbf{b}] \log \mathcal{Z}[\mathbf{m}, \mathbf{b}] \end{aligned} \quad (32)$$

Thus, the coherent information takes the simple form

$$\begin{aligned} I^{(c)}(Q : R; \mathcal{E}) &= 2 \log N + \sum_{\mathbf{e}, \mathbf{a}} \mathcal{Z}[\mathbf{e}, \mathbf{a}] \log \frac{\mathcal{Z}[\mathbf{e}, \mathbf{a}]}{\sum_{\mathbf{a}'} \mathcal{Z}[\mathbf{e}, \mathbf{a}']} \\ &\quad + \sum_{\mathbf{m}, \mathbf{b}} \mathcal{Z}[\mathbf{m}, \mathbf{b}] \log \frac{\mathcal{Z}[\mathbf{m}, \mathbf{b}]}{\sum_{\mathbf{b}'} \mathcal{Z}[\mathbf{m}, \mathbf{b}']} \end{aligned} \quad (33)$$

We can view these expressions as disorder averages over frustration variables  $\mathbf{e}$  and  $\mathbf{m}$ . Since the disorder distribution is precisely given by the partition function, the model falls on the Nishimori line [87, 88]. The Nishimori line is very special because the disordered model acquires an effective local  $\mathbb{Z}_N$  symmetry. This is unsurprising in our context, since the partition functions are describing spectra of density matrices in a gauge theory.

Furthermore, note that the ratios  $P[\mathbf{a}|\mathbf{e}] = \frac{\mathcal{Z}[\mathbf{e}, \mathbf{a}]}{\sum_{\mathbf{a}'} \mathcal{Z}[\mathbf{e}, \mathbf{a}']}$  and  $P[\mathbf{a}|\mathbf{m}] = \frac{\mathcal{Z}[\mathbf{m}, \mathbf{a}]}{\sum_{\mathbf{a}'} \mathcal{Z}[\mathbf{m}, \mathbf{a}']}$  correspond to winding number probabilities conditioned on the disorder realization. Therefore,  $I^{(c)}(Q : R; \mathcal{E})$  can equivalently be expressed as

$$I^{(c)}(Q : R; \mathcal{E}) = 2 \log N - [H(\mathbf{a}|\mathbf{e})] - [H(\mathbf{b}|\mathbf{m})] \quad (34)$$

where  $H(\mathbf{a}|\mathbf{e})$  and  $H(\mathbf{b}|\mathbf{m})$  denote Shannon entropies of the conditional distributions  $P[\mathbf{a}|\mathbf{e}]$  and  $P[\mathbf{b}|\mathbf{m}]$  respectively, and  $[\dots]$  denotes a disorder average on the Nishimori line. This final expression for the coherent information is particularly well suited for numerical evaluation.

### 2. Conditional Mutual Information

To compute the conditional mutual information, we need to work with reduced density matrices. Consider the Toric code logical state  $|\Psi_0\rangle$  subject to only  $X$  type dephasing. In Appendix B, we show that the conditional mutual information for the geometry illustrated in (21) reduces to the following simple form.

$$\begin{aligned} I(A : C|B) &= - \sum_{\mathbf{e}_{AB}} \mathcal{Z}[\mathbf{e}_{AB}] \log \mathcal{Z}[\mathbf{e}_{AB}] \\ &\quad - \sum_{\mathbf{e}_{BC}, E_A} \mathcal{Z}[\mathbf{e}_{BC}, E_A] \log \mathcal{Z}[\mathbf{e}_{BC}, E_A] \\ &\quad + \sum_{\mathbf{e}_B, E_A} \mathcal{Z}[\mathbf{e}_B, E_A] \log \mathcal{Z}[\mathbf{e}_B, E_A] \\ &\quad + \sum_{\mathbf{e}_{ABC}} \mathcal{Z}[\mathbf{e}_{ABC}] \log \mathcal{Z}[\mathbf{e}_{ABC}] \end{aligned} \quad (35)$$

Here  $\mathbf{e}_Q = \{e_v | v \in \text{Int}(Q)\}$  denotes the electric charges within region  $Q$ , excluding the boundary  $\partial Q$ . We define the reduced partition function on region  $Q$  by summing over all charge configurations outside  $Q$ :  $\mathcal{Z}[\mathbf{e}_Q] = \sum_{\mathbf{e}_{v \notin \text{Int}(Q)}} \mathcal{Z}[\mathbf{e}]$ . Furthermore, we define the total charge enclosed by region  $Q$  as  $E_Q = \sum_{v \in \text{Int}(Q)} e_v$ . Since regions  $B$  and  $BC$  are annular geometries, their associated partition functions depend on the total charge contained inside the hole which is precisely given by  $E_A$ .

In Appendix C, we also consider the relative entropy of two decohered logical states and express it in terms of conditional winding number distributions.

### E. Random Bond Clock Models

In the previous section, we expressed all relevant quantities in terms of  $\mathcal{Z}[\mathbf{e}, \mathbf{a}]$  and  $\mathcal{Z}[\mathbf{m}, \mathbf{a}]$ . We now demonstrate that these quantities can be interpreted as partition functions of classical two-dimensional spin models.

First let us parametrize the variables  $\{p_k^{x,z}\}$  as follows  $p_k^{x,z} = e^{\alpha_k^{x,z}} / \mathcal{N}_{x,z}$  where  $\mathcal{N}_{x,z} = \sum_{k=0}^{N-1} e^{\alpha_k^{x,z}}$ . Next, we introduce the discrete Fourier transform of  $\{\alpha_k^{x,z}\}$  as

$$\beta_m^{x,z} = \frac{1}{N} \sum_{k=0}^{N-1} \alpha_k^{x,z} \omega^{-km} \quad , \quad \alpha_k^{x,z} = \sum_{m=0}^{N-1} \beta_m^{x,z} \omega^{km} \quad (36)$$

Now, consider the quantity:

$$\mathcal{Z}[\mathbf{e}, \mathbf{a}] = \sum_{\substack{(\nabla \cdot \mathbf{k}^x)_v = e_v \\ \hat{\mathcal{C}}(\mathbf{k}^x) = \mathbf{a}}} \prod_{\mu} p_{k_\mu}^x \quad (37)$$

We need to parameterize all the  $\mathbf{k}^x$  “flow” configurations which solve the constraints  $(\nabla \cdot \mathbf{k}^x)_v = e_v$  and  $\hat{\mathcal{C}}(\mathbf{k}^x) = \mathbf{a}$ .  $\mathbf{k}^x$  consists of  $2L^2$  qudit degrees of freedom on the links but they are subject to  $L^2 + 1$  constraints ( $L^2 - 1$  independent divergence constraints and 2 homology constraints

along the 2 non-contractible cycles of the torus). That leaves  $2L^2 - (L^2 + 1) = L^2 - 1$  independent qudit degrees of freedom. Now let  $k_{\mu, \mathbf{a}}^e$  denote a reference configuration which solves  $(\nabla \cdot \mathbf{k}_\mathbf{a}^e)_v = e_v$  and  $\hat{\mathcal{C}}(\mathbf{k}_\mathbf{a}^e) = \mathbf{a}$ . All other flow configurations are related to this reference configuration via additional closed, contractible Wilson loops, namely  $\mathbf{k}^x = \mathbf{k}_\mathbf{a}^e + \mathbf{l}^x$  where  $(\nabla \cdot \mathbf{l}^x)_v = 0$  and  $\hat{\mathcal{C}}(\mathbf{l}^x) = 0$ . One convenient way to parameterize the set of all  $\mathbf{l}^x$  configurations is to introduce  $\mathbb{Z}_N$  spins  $\theta_p$  at the center of each plaquette  $p$  and write

$$l_{\mu \perp \langle p_1 \rightarrow p_2 \rangle}^x = \theta_{p_1} - \theta_{p_2} \pmod{N} \quad (38)$$

where  $\langle p_1 \rightarrow p_2 \rangle$  denotes the unique dual lattice link from  $p_1$  to  $p_2$  which intersects the direct lattice link  $\mu$ . We stick to the orientation convention that if a direct lattice link goes from bottom to top, the unique dual link which intersects it crosses it from left to right. Now for any configuration of spins  $\{\theta_p\}$ , we have  $(\nabla \cdot \mathbf{l}^x)_v = 0$  and  $\hat{\mathcal{C}}(\mathbf{l}^x) = 0$ .  $\{l_\mu^x\}$  are precisely interpreted as domain walls between neighboring spin configurations. Furthermore, since  $l_\mu^x$  is unchanged by the global shift  $\theta_p \rightarrow (\theta_p + a) \pmod{N}$  where  $a = 0, \dots, N-1$ , we obtain precisely  $L^2 - 1$  independent qudit degrees of freedom. In terms of the spins  $\{\theta_p\}$ ,  $\mathcal{Z}[\mathbf{e}, \mathbf{a}]$  can be written as the partition function of a spin model on the dual lattice with nearest-neighbor interactions and quenched bond disorder given by  $\hat{k}_{\mu; \mathbf{a}}^e$ .

$$\mathcal{Z}[\mathbf{e}, \mathbf{a}] = \frac{1}{\mathcal{N}_x^{2L^2}} \sum_{\{\theta_p\}} \exp\{-H[\{\theta_p\}; \mathbf{k}_\mathbf{a}^e]\} \quad (39)$$

$$H[\{\theta_p\}; \mathbf{k}_\mathbf{a}^e] = - \sum_{\langle p \rightarrow p' \rangle} \sum_{m=0}^{N-1} \beta_m^x \omega^{m(\hat{k}_{\langle p \rightarrow p' \rangle, \mathbf{a}}^e + \theta_p - \theta_{p'})} \quad (40)$$

The parameters  $\beta_m^x$  correspond to coupling constants that source distinct harmonic interactions in the spin model. For generic choices of  $\beta_m^x$ , the model suffers from a sign problem. However, for charge conjugation symmetric channels, this obstruction is lifted since only cosine harmonics survive and the resulting Boltzmann weights become positive definite.

$$H[\{\theta_p\}; \mathbf{k}_\mathbf{a}^e] = - \sum_{\langle p, p' \rangle} \sum_{m=0}^{[N/2]} \beta_m^x \times \cos\left(\frac{2\pi m(k_{\langle p, p' \rangle, \mathbf{a}}^e + \theta_p - \theta_{p'})}{N}\right) \quad (41)$$

This is now the Hamiltonian for a random phase clock model (a “discrete gauge glass”) with coupling constants  $\beta_m^x$  which source different cosine harmonics. The vertex charges  $e_v$  become local bond frustrations on the dual lattice  $(\nabla \times \hat{\mathbf{k}}_\mathbf{a}^e)_p = e_p \pmod{N}$ . In particular, if  $e_p \neq 0$ , no configuration of the clock spins can simultaneously minimize all interactions around the corresponding plaquette, signaling local frustration. Note

that these frustrations are the only “gauge invariant components” of the quenched disorder since the partition function is invariant under the “gauge transformation”  $\hat{k}_{\langle p \rightarrow p' \rangle, \mathbf{a}}^e \rightarrow \hat{k}_{\langle p \rightarrow p' \rangle, \mathbf{a}}^e + \alpha_p - \alpha_{p'}$ . Finally note that the logical eigenvalues  $\mathbf{a} = (a_1, a_2)$  impose twisted boundary conditions along the non-contractible cycles of the torus. These twists introduce global, topological frustrations in the clock model, leading to different statistical weights for each winding number sector.

Similarly now consider the quantity:

$$\mathcal{Z}[\mathbf{m}, \mathbf{a}] = \sum_{\substack{(\nabla \times \mathbf{k}_\mathbf{a}^z)_p = m_p \\ \mathcal{C}(\mathbf{k}_\mathbf{a}^z) = \mathbf{a}}} \prod_{\mu} p_{k_\mu^z}^z \quad (42)$$

Once again,  $\mathbf{k}^z$  involves  $2L^2$  link degrees of freedom and is subject to  $L^2 + 1$  independent constraints ( $L^2 - 1$  independent curl constraints and the two global homology constraints associated with the noncontractible cycles of the torus). This leaves  $L^2 - 1$  independent qudit degrees of freedom. Let  $k_{\mu; \mathbf{a}}^m$  denote a fixed reference configuration which satisfies  $(\nabla \times \mathbf{k}_\mathbf{a}^m)_p = m_p$  and  $\mathcal{C}(\mathbf{k}_\mathbf{a}^m) = \mathbf{a}$ . All other configurations are now related to this reference configuration by the action of closed, contractible ’t Hooft loops, namely  $\mathbf{k}^z = \mathbf{k}_\mathbf{a}^m + \mathbf{l}^z$  where  $(\nabla \times \mathbf{l}^z)_p = 0$  and  $\mathcal{C}(\mathbf{l}^z) = 0$ . Again a convenient way to parametrize the full set of  $\mathbf{k}^z$  configurations is to introduce  $\mathbb{Z}_N$ -valued spin variables  $\theta_v$  residing on the vertices  $v$ , and define

$$l_{\mu = \langle v_1 \rightarrow v_2 \rangle}^z = \theta_{v_1} - \theta_{v_2} \pmod{N} \quad (43)$$

Now, for any configuration of spins  $\{\theta_v\}$ , we have  $(\nabla \times \mathbf{l}^z)_p = 0$  and  $\mathcal{C}(\mathbf{l}^z) = 0$ . Furthermore, since  $l_\mu^z$  is unchanged by the global shift  $\theta_v \rightarrow (\theta_v + b) \pmod{N}$  where  $b = 0, \dots, N-1$ , this parametrization yields precisely  $L^2 - 1$  independent qudit degrees of freedom. In terms of spin variables  $\{\theta_v\}$ ,  $\mathcal{Z}[\mathbf{m}, \mathbf{a}]$  becomes a partition function of a clock model on the direct lattice with nearest-neighbor interactions and quenched bond disorder specified by the reference configuration  $k_{\mu; \mathbf{a}}^m$ .

$$\mathcal{Z}[\mathbf{m}, \mathbf{a}] = \frac{1}{\mathcal{N}_z^{2L^2}} \sum_{\{\theta_v\}} \exp\{-H[\{\theta_v\}; \mathbf{k}_\mathbf{a}^m]\}$$

$$H[\{\theta_v\}; \mathbf{k}_\mathbf{a}^m] = \sum_{\langle v \rightarrow v' \rangle} \sum_{n=0}^{N-1} \beta_n^z \omega^{n(k_{\langle v \rightarrow v' \rangle, \mathbf{a}}^m + \theta_v - \theta_{v'})} \quad (44)$$

Once again, the parameters  $\beta_n^z$  act as coupling constants that source distinct harmonic interactions in the spin model. Assuming charge conjugation symmetry of the channel again reduces this to the disordered cosine clock model. The magnetic fluxes  $m_p$  now correspond to local frustration variables.

We have shown above that the spectra of the decohered density matrices can be expressed in terms of partition functions of 2D disordered clock models. Since the evaluation of information theoretic measures reduces to computing disorder averaged expectation values of nonlinear

functions of these partition functions along the Nishimori line, the problem of characterizing mixed state phases of the decohered  $\mathbb{Z}_N$  Toric code essentially reduces to understanding the thermodynamic phases of the associated disordered clock models on the Nishimori line.

$\mathbb{Z}_N$  clock models in two dimensions have been studied extensively in the literature. Notable special cases include the Ising model ( $N = 2$ ), three-state Potts model ( $N = 3$ ), the Ashkin-Teller model ( $N = 4$ ) and the XY model ( $N \rightarrow \infty$ ). These models possess a dihedral symmetry  $D_N = \mathbb{Z}_N \rtimes \mathbb{Z}_2^P$  and, in the absence of disorder, they are known to display a rich phase diagram that changes qualitatively with increasing  $N$ . In particular, for  $2 \leq N \leq 4$ , the  $\mathbb{Z}_N$  clock model exhibits only two phases: a low temperature ordered phase and a high temperature disordered phase. These two phases are separated by a single critical point. On the other hand, for  $N > 4$ , the  $\mathbb{Z}_N$  clock model is found to exhibit three different phases: a low temperature ordered phase, a high temperature disordered phase, and an intervening quasi-long-range-ordered (QLRO) critical phase [59–62, 89–94]. Within this intermediate phase, both the domain wall and vortex excitations are RG irrelevant, and the IR effective theory becomes Gaussian with an emergent  $U(1)$  symmetry. Crucially, because the low-energy excitations in this phase are gapless spin wave modes, the correlation length diverges throughout the phase. The existence of such a QLRO phase follows from general renormalization group arguments, and it does not rely on any fine-tuned choice of coupling constants. Microscopic couplings merely affect nonuniversal properties, such as the exact locations of the critical points, but they do not alter the qualitative structure of the phase diagram.

In the presence of the quenched phase disorder, the fate of the intermediate QLRO phase becomes uncertain [95]. Indeed, it is known that sufficiently strong disorder completely destroys all signatures of the QLRO phase. However, when restricted to the Nishimori line, it is generally expected that the qualitative structure of the phase diagram mirrors that of the clean  $\mathbb{Z}_N$  clock model [63, 64]. In the next section, we verify numerically that this is indeed the case. Precisely which phase the decohered Toric code occupies ultimately depends on the decoherence channels and the choice of parameters  $p_k^{x,z}$ . In the next section, we make a concrete choice for these parameters and numerically confirm the emergence of all three phases along the Nishimori line for  $N > 4$ . We then examine the implications of these phases for the information-theoretic measures introduced above. Note that a similar analysis was carried out for measurement-induced phases in symmetric quantum circuits [96].

### III. INFORMATION CRITICAL PHASES

In this section, we define the information critical phase, and demonstrate that such a phase arises in decohered  $\mathbb{Z}_N$  Toric codes for  $N > 4$ .

#### A. Intrinsic mixed-state behavior

It is instructive to compare the CMI with the ordinary mutual information (MI) between regions  $A$  and  $C$ ,

$$I(A : C) := S(A) + S(C) - S(AC) \quad (45)$$

The MI upper-bounds all connected correlators of operators supported on  $A$  and  $C$ :

$$\frac{1}{2} \left( \frac{\langle O_A O_B \rangle_c}{\|O_A\| \cdot \|O_B\|} \right)^2 \leq I(A : C), \quad (46)$$

where  $\langle \cdot \rangle_c$  denotes the connected correlation function, and  $\|O\| := \max_{\psi} \sqrt{\langle \psi | O^\dagger O | \psi \rangle}$  is an operator norm. In a short-range correlated phase, the MI typically decays with the separation  $r := \text{dist}(A, C)$  as

$$I(A : C) \sim \text{poly}(|A|, |C|) e^{-r/\xi}, \quad (47)$$

where  $\xi$  is just the familiar correlation length. This behaviour causes all connected correlators to also decay exponentially on the same length scale  $\xi$ . Divergence of  $\xi$  signals conventional criticality, where power-law correlations may emerge.

Interestingly, if  $\xi_M = \infty$  but  $\xi < \infty$ , we obtain a different kind of criticality that does not require long-range two-point correlations. This separation between the behaviors of  $I(A : C)$  and  $I(A : C|B)$  is an *intrinsically mixed-state phenomenon*. To see this, imagine that  $ABC$  is pure, then, we find that

$$I(A : C) = I(A : C|B) \quad (\text{for pure states}). \quad (48)$$

Consequently, correlation and Markov lengths must diverge together at pure-state critical points and separation of scales between  $\xi_M$  and  $\xi$  must be a genuine mixed state phenomenon. Known examples of this such information criticality are decoherence-induced critical points of the  $\mathbb{Z}_2$  Toric code where  $\xi = 0$  but  $\xi_M = \infty$ .

In the context of pure state phases, one may encounter not only isolated quantum critical points, but also quantum critical phases, which are contiguous regions in phase space characterized by a diverging correlation length. By analogy, we now define an *information critical phase* as an extended region in phase space characterized by a diverging Markov length ( $\xi_M = \infty$ ) but a finite correlation length ( $\xi < \infty$ ).

This definition ensures that this phase exhibits stability against certain (symmetry respecting) perturbations upto a finite threshold, thereby distinguishing it from an isolated information critical point. While we do not assume any additional structure, such as emergent conformal invariance or a continuous manifold of renormalization group fixed points, in defining an information critical phase, it is natural to wonder whether analogous features may nevertheless emerge.

We now study the mixed-state phase diagram of the  $\mathbb{Z}_N$  toric code under decoherence, and present evidence for an *information critical phase* when  $N > 4$ .

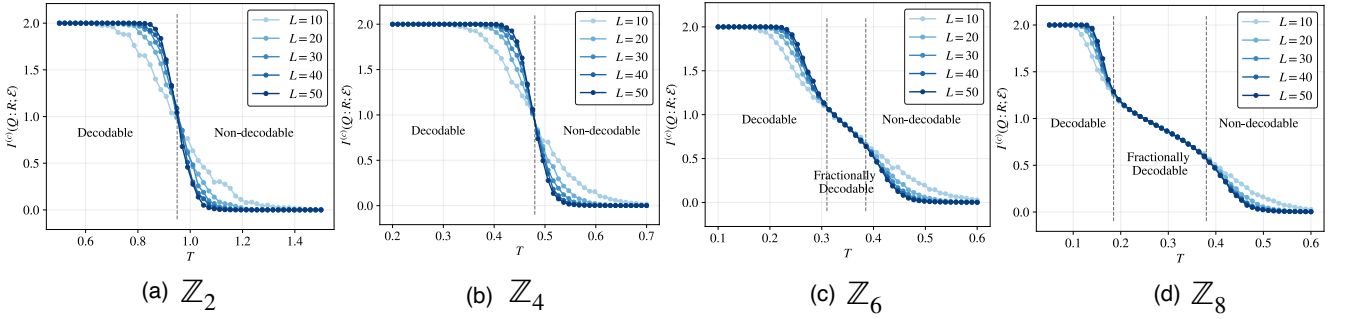


**FIG. 3. Coherent Information.** We numerically compute the coherent information of the  $\mathbb{Z}_N$  toric code for  $N = 2, 4, 6$ , and  $8$  under  $X$ -type dephasing.  $L$  denotes the linear size of the Toric code. The decoherence parameters  $p_k^x$  are fixed as in Eq. (49) with the decoherence temperature  $T \equiv T^x$  acting as the sole control parameter. To enable a direct comparison across different values of  $N$ , the vertical axis is plotted in logarithmic units of base  $N$ . For  $N \leq 4$ , we observe a single phase transition in the disordered clock model, separating an ordered and a disordered phase. In the ordered phase, the coherent information saturates to  $2 \log N$ , indicating perfect decodability of the encoded logical information. In contrast, in the disordered phase the coherent information vanishes in the thermodynamic limit, signaling the complete loss of encoded quantum information. For  $N > 4$ , however, the corresponding clock model exhibits three distinct phases: an ordered phase, a disordered phase, and an intervening QLRO phase. Remarkably, within the QLRO phase the coherent information saturates to a nonzero fractional value of  $2 \log N$  as  $L \rightarrow \infty$ , indicating that a finite fraction of logical information is still protected. The extent of this fractionally decodable phase grows with increasing  $N$ , and we find that the second critical temperature  $T_c^{(2)} \sim 0.38$  is approximately independent of the value of  $N$ . Interestingly, the locations of the critical points are found to agree to excellent precision with the self-dual identity given in Eq. (55).

## B. Numerical details

For convenience, we choose the  $X$  and  $Z$  decoherence parameters to take the form

$$p_k^{x,z} = \frac{1}{\mathcal{N}^{x,z}} \exp\left(\frac{1}{T^{x,z}} \cos \frac{2\pi k}{N}\right), \quad (49)$$

where  $\mathcal{N}^{x,z}$  is a normalization constant. The sole control parameter in this choice is the effective *decoherence temperature*  $T^{x,z}$ , which sets the strength of the noise. For small  $T^{x,z}$ , the distribution  $p_k^{x,z}$  is sharply peaked around  $k = 0$ , corresponding to weak decoherence. In contrast, for large  $T^{x,z}$  the distribution becomes approximately uniform,  $p_k^{x,z} \simeq 1/N$ , corresponding to the strong-decoherence limit. In the notation of Eq. (41), the above choice corresponds to retaining just the first non-trivial cosine harmonic with coupling  $\beta_1^{x,z} = 1/T^{x,z}$ . All higher harmonics  $\beta_m^{x,z}$  are set to zero.

Here we briefly outline some numerical details. Throughout, we restrict attention to  $X$ -type dephasing, since the treatment of  $Z$ -type dephasing is entirely analogous. This exclusively sources electric charge excitations. Recall that the coherent information requires evaluating the conditional winding number distribution  $P[\mathbf{a}|\mathbf{e}] = \frac{\mathcal{Z}[\mathbf{e}, \mathbf{a}]}{\sum_{\mathbf{a}'} \mathcal{Z}[\mathbf{e}, \mathbf{a}']}$ . We compute this quantity efficiently using the worm algorithm [97–99], which directly samples configurations in the current-loop expansion of the disordered clock model, as given in Eq. (37). Because we work with disordered clock models, we begin by parametrizing the allowed flow configuration  $\mathbf{k}$  as  $\mathbf{k} = \mathbf{k}' + \mathbf{l}$  where the reference configuration  $\mathbf{k}'$  satisfies the required divergence constraints, namely  $(\nabla \cdot \mathbf{k}')_v = e_v$ . Having

fixed the reference configuration, the fluctuation  $\mathbf{l}$  must be divergence free, namely  $(\nabla \cdot \mathbf{l})_v = 0$ . Such divergence-free configurations are efficiently sampled by sequentially adding closed loops (“worms”) of charge. The worm algorithm temporarily relaxes the divergence constraint by introducing a pair of defects—the head and tail of the worm—which locally violate charge conservation. The Markov chain then propagates the head via local updates weighted by the Boltzmann factor, with modified statistical weights  $\prod_\mu p_{k'_\mu + l_\mu}$ . When the head returns to the tail, the defects annihilate, and the configuration once again satisfies the constraints of the original model. Ordinary expectation values are obtained by averaging exclusively over closed-worm configurations, while the intermediate open-worm configurations enable the evaluation of defect correlation functions. Importantly, the worm algorithm exhibits minimal critical slowing down and is ergodic across all topological sectors [97–99], making it particularly well suited for computing the conditional winding-number probabilities  $P[\mathbf{a}|\mathbf{e}]$  at fixed backgrounds of charges. Finally, since our ultimate interest lies in disorder averaged observables along the Nishimori line, the reference configurations  $\mathbf{k}'$  may be sampled directly from the product distribution  $p(\mathbf{k}') = \prod_\mu p_{k'_\mu}$ .

We now discuss the resulting phase diagram of the  $X$ -decohered Toric code, highlighting the qualitative differences between the cases  $N \leq 4$  and  $N > 4$ .

## C. $N \leq 4$

For  $N \leq 4$ , the random bond clock model exhibits only 2 distinct phases: a low-temperature ordered phase and a

high-temperature disordered phase. The Markov length remains finite in each phase, and consequently the CMI exhibits exponential decays in the thickness of  $B$

$$I(A : C|B) \sim e^{-r/\xi_M(T^x)} \quad (50)$$

Furthermore, in the ordered phase, topological tunneling processes are exponentially suppressed in the system size. As a result, the conditional winding number distribution  $P[\mathbf{a}|\mathbf{e}]$  is up to exponentially small corrections sharply peaked at  $\mathbf{a} = 0$ . This implies that  $[H(\mathbf{a}|\mathbf{e})] \approx 0$  and hence the coherent information remains approximately maximal.

$$I^{(c)}(Q : R; \mathcal{E}) \approx 2 \log N + \mathcal{O}(e^{-\alpha L}) \quad (51)$$

The system therefore realizes a decodable phase in which logical information remains asymptotically perfectly protected in the thermodynamic limit ( $L \rightarrow \infty$ ). On the other hand, in the disordered phase the free energy cost of system spanning loops vanishes, leading to uniform sampling over all topological sectors. This implies that  $P[\mathbf{a}|\mathbf{e}] \approx \frac{1}{N^2}$ , yielding,

$$I^{(c)}(Q : R; \mathcal{E}) \approx 0 + \mathcal{O}(e^{-\alpha' L}) \quad (52)$$

Consequently, all logical quantum information is destroyed in this regime, and the system can function at most as a classical memory. These expectations are borne out numerically in Fig. 3 for the  $\mathbb{Z}_2$  and  $\mathbb{Z}_4$  Toric code. Crucially, note that at the critical point, the coherent information becomes independent of system size  $L$  indicating emergent scale invariance. This is a consequence of the fact that the disordered clock model is at criticality and exhibits power law correlations. In this regime, the Markov length diverges ( $\xi_M = \infty$ ) and the CMI decays only algebraically. This is a genuine mixed state phase transition of the decohered Toric code.

#### D. $N > 4$

When  $N > 4$ , the phenomenology of the ordered and disordered phases remains qualitatively identical to when  $N \leq 4$ . These phases continue to correspond to decodable and non-decodable phases respectively, both characterized by a finite Markov length. However, in the intermediate QLRO phase, the clock model becomes scale invariant, signaling a divergent Markov length ( $\xi_M = \infty$ ) over an extended region of the phase diagram. We identify this as an information critical phase.

The emergent scale invariance also manifests directly in the behavior of the coherent information, which becomes independent of the system size  $L$  across this phase and saturates to a finite, fractional value in the thermodynamic limit. The appearance of this fractional plateau indicates the persistence of a partially protected logical subspace.

In the clean clock model, the QLRO phase is governed in the infrared by a Gaussian spin-wave theory, and the two phase boundaries are of Berezinskii–Kosterlitz–Thouless (BKT) type. Along the Nishimori line in the disordered case, we again expect the effective low energy theory to be Gaussian, but with a stiffness renormalized by bulk disorder. Distinct topological sectors in this phase are connected by harmonic zero modes winding around the torus. As shown in Appendix D, the energies of these winding modes are independent of system size, leading to conditional winding number probabilities of the form

$$P(\mathbf{a}|\mathbf{e}) \sim e^{-\frac{\kappa(T^x)}{2} |\mathbf{a}|^2} \quad (53)$$

where  $\kappa(T^x)$  is the renormalized spin stiffness, which depends on the decoherence strength, and  $\mathbf{a}$  is now shifted to the symmetric integer range  $\{-\lfloor N/2 \rfloor, \dots, \lfloor N/2 \rfloor\}$ . Note that despite being independent of system size, these probabilities remain exponentially suppressed in the topological charge  $\mathbf{a}$ . These expectations are borne out numerically in Fig. 3 for the  $\mathbb{Z}_6$  and  $\mathbb{Z}_8$  Toric code. We observe from our numerics that the second critical point  $T_c^{(2)} \approx 0.38$  is approximately independent of  $N$  just as for the clean clock model.

In Appendix D 2, we employ a Gaussian spin-wave ansatz to provide a qualitative explanation for the saturation of the conditional mutual information in the QLRO phase and the resulting divergence of the Markov length in this regime.

#### E. Critical points and self-duality

The robustness of logical information encoded in the  $\mathbb{Z}_N$  Toric code can be contrasted with a minimal setting involving two raw qudits subject to independent  $X$  and  $Z$  dephasing channels, characterized by effective temperatures  $T^x$  and  $T^z$ . The coherent information of this two-qudit system is given by

$$I_{\text{raw}}^{(c)} = 2 \left( \log N - \sum_{i=x,z} H(T^i) \right), \quad (54)$$

where  $H(T^i) = -\sum_{k=0}^{N-1} p_k^i(T^i) \log p_k^i(T^i)$  is the Shannon entropy of the distributions  $p_k^i(T^i)$  defined in Eq. (49).

In the case of the Toric code, the coherent information remains fixed at its maximal value  $2 \log N$  up to a finite threshold  $T^i \leq T_c^{(1)}$ , reflecting the intrinsic robustness afforded by topological encoding. In contrast, for the raw qudits the coherent information degrades continuously as the noise strength  $T^i$  is increased. For  $N = 2$ , it is well known that the numerically observed error threshold  $T_c$  (or equivalently  $p_c$ ) of the Toric code is, to an excellent approximation, determined by setting  $T^x = T^z$  and finding the point where  $I_{\text{raw}}^{(c)} = 0$ . This coincides with the asymptotic Gilbert–Varshamov bound for CSS-type codes [2, 84].

We find that the same equation,  $\log N = 2H(T_c)$ , continues to predict the location of the critical point  $T_c$  at which the coherent information  $I^{(c)}(Q : R; \mathcal{E})$  undergoes a transition to excellent precision for all  $N \leq 4$ . Even more remarkably, for  $N > 4$ , where two distinct phase transitions appear at  $T_c^{(1)}$  and  $T_c^{(2)}$ , both critical points obey the self-duality relation given by  $I_{\text{raw}}^{(c)} = 0$ :

$$\log N = H(T_c^{(1)}) + H(T_c^{(1)}). \quad (55)$$

While we are unable to provide a information-theoretic explanation for this fact at this stage, we note that the same relation has previously appeared as a conjectured self-duality condition for disordered spin models along the Nishimori line [100–105]. These observations reveal a deep link between self-duality in disordered spin systems along the Nishimori line and the error thresholds of topological quantum error-correcting codes.

#### IV. SEPARABILITY TRANSITIONS

In the  $\mathbb{Z}_2$  Toric code, it is known that within the non-decodable phase, the decohered density matrix can be written as a convex combination of short-range entangled (SRE) pure states [53]. By contrast, in the decodable phase, no such decomposition is expected to exist, as the state retains long-range entanglement, as diagnosed by the topological entanglement negativity [26]. The transition between these two regimes is known as a decoherence-induced *separability transition*.

In the  $\mathbb{Z}_{N>4}$  Toric code, it is natural to ask how separability should be understood within the information critical phase. We now show that in the information critical phase, the mixed state admits a decomposition as a convex combination of “Coulombic” pure states. These pure states support gapless gauge modes, which we interpret as emergent photons. This observation establishes a connection between information critical mixed states and conventional quantum critical pure states.

Following Refs. [41, 53, 65], we employ the “minimally entangled typical thermal state” (METTS) ansatz to express the  $X$ -dephased Toric code density matrix, initialized in state  $|\Psi_0\rangle$ , as the following convex ensemble of pure states

$$\begin{aligned} \mathcal{E}(\rho_Q) &= \sum_{\mathbf{x}} \mathcal{E}(\rho_Q)^{1/2} |\mathbf{x}\rangle \langle \mathbf{x}| \mathcal{E}(\rho_Q)^{1/2} \\ &= \sum_{\mathbf{x}} |\psi_Q(\mathbf{x})\rangle \langle \psi_Q(\mathbf{x})| \end{aligned} \quad (56)$$

Here  $|\mathbf{x}\rangle = |\{x_\mu\}\rangle$  denotes simultaneous eigenstates of all Pauli  $X$  operators. Each METTS wavefunction  $|\psi_Q(\mathbf{x})\rangle$  is obtained by “modular evolution” of the product state  $|\mathbf{x}\rangle$  by the operator  $\mathcal{E}(\rho_Q)^{1/2}$ . Such a decomposition has proven to be tremendously useful in the  $\mathbb{Z}_2$  Toric code since the states  $|\psi_Q(\mathbf{x})\rangle$  undergo a phase transition from topologically ordered to topologically trivial precisely at the decodability threshold.

Since we only consider  $X$ -type dephasing, the plaquette stabilizer constraint  $B_p = 1$  is never violated. Consequently, the decohered density matrix has support only on  $|\mathbf{x}\rangle$  configurations satisfying  $B_p |\mathbf{x}\rangle = |\mathbf{x}\rangle$  for all plaquettes  $p$ . But all such configurations can be constructed from the reference state  $|\mathbf{1}\rangle \equiv |\{x_\mu = 1\}\rangle$  by acting with closed ‘t Hooft loops:  $|\mathbf{x}\rangle = Z_{\mathcal{C}(\mathbf{x})} |\mathbf{1}\rangle$ . Because these loop operators commute with  $\mathcal{E}(\rho_Q)$ , the corresponding METTS states satisfy  $|\psi_Q(\mathbf{x})\rangle = Z_{\mathcal{C}(\mathbf{x})} |\psi_Q(\mathbf{1})\rangle$ . Thus, all  $|\psi_Q(\mathbf{x})\rangle$  are related by finite-depth local unitaries and therefore lie in the same quantum phase. To diagnose their topological character, it is therefore sufficient to analyze the reference state  $|\psi_Q(\mathbf{1})\rangle$ .

Using the explicit form of the decohered density matrix, one finds

$$|\psi_Q(\mathbf{1})\rangle = \sum_{\mathbf{z}} \mathcal{Z}[\mathbf{z}]^{1/2} |\mathbf{z}\rangle \quad (57)$$

where  $|\mathbf{z}\rangle = |\{z_\mu\}\rangle$  denotes simultaneous eigenstates of all Pauli  $Z$  operators and

$$\mathcal{Z}[\mathbf{z}] = \sum_{\substack{(\nabla \cdot \mathbf{k})_v = 0 \\ \mathcal{C}(\mathbf{k}) = 0}} \prod_{\mu} p_{k_\mu - z_\mu}^x \quad (58)$$

is again the classical partition function of a disordered clock model with quenched couplings  $\mathbf{z}$ . In the low-temperature (weak-decoherence) limit, one has  $|\psi_Q(\mathbf{1})\rangle \propto |\Psi_0\rangle$ , and the state retains full topological order. In contrast, in the high-temperature (strong-decoherence) limit,  $|\psi_Q(\mathbf{1})\rangle \propto |\{x_\mu = 1\}\rangle$  which is a trivial product state.

A convenient diagnostic of topological order is the expectation value of a non-contractible Wilson loop  $X_{\mathcal{C}}^q$  carrying charge  $q = 1, \dots, N-1$  with respect to the state  $|\psi_Q(\mathbf{1})\rangle$ . Physically,  $\langle X_{\mathcal{C}}^q \rangle$  measures the amplitude for tunneling between distinct topological sectors of the  $\mathbb{Z}_N$  Toric code. This amplitude vanishes in a topologically ordered phase, while it saturates to an  $\mathcal{O}(1)$  value in a topologically trivial phase where anyons condense. Since  $X_{\mathcal{C}} |\mathbf{z}\rangle = |\mathbf{z} + q\delta_{\mathcal{C}}\rangle$  where the delta function  $\delta_{\mathcal{C}}$  is only non-zero along the links belonging to the loop  $\mathcal{C}$ , we find that

$$\begin{aligned} \langle X_{\mathcal{C}}^q \rangle &= \sum_{\mathbf{z}} \sqrt{\mathcal{Z}[\mathbf{z}] \mathcal{Z}[\mathbf{z} + q\delta_{\mathcal{C}}]} \\ &= \sum_{\mathbf{z}} \mathcal{Z}[\mathbf{z}] \sqrt{\frac{\mathcal{Z}[\mathbf{z} + q\delta_{\mathcal{C}}]}{\mathcal{Z}[\mathbf{z}]}} \end{aligned} \quad (59)$$

which can be interpreted as a Nishimori line expectation of a ratio of conditional winding number probabilities:  $\langle X_{\mathcal{C}}^q \rangle = [\sqrt{P(q|\mathbf{z})/P(0|\mathbf{z})}]$ . This quantity can be evaluated numerically using the same Monte-Carlo techniques introduced in Sec. III B. The resulting behavior for the decohered  $\mathbb{Z}_8$  Toric code is shown in Fig. 4.

As expected, in the decodable phase the expectation value decays exponentially with system size, whereas in

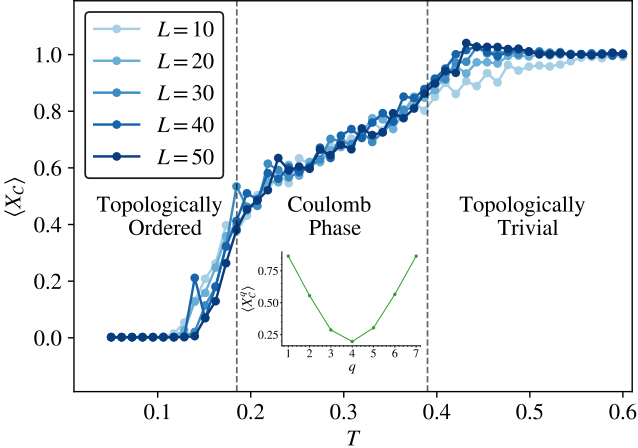


**FIG. 4. Wilson Loop Expectation.** We plot the expectation value of the Wilson loop operator  $\langle X_C^q \rangle$  (shown here for  $q = 1$ ) with respect to the METTS wavefunction  $|\psi_Q(1)\rangle$  (Eq. (57)) as a function of the decoherence temperature for the  $\mathbb{Z}_8$  Toric code. In the decodable phase,  $\langle X_C^q \rangle$  vanishes in the thermodynamic limit, signaling topological order, whereas in the non-decodable phase it saturates to 1 indicating topological triviality. In the information critical phase,  $\langle X_C^q \rangle$  approximately saturates to a constant that is roughly independent of system size and increases monotonically with decoherence strength. The inset shows the dependence of this saturation value on the loop charge  $q \bmod N$  within the information critical phase (at  $T = 0.3$ ). We find that the saturation is sharply decreasing with increasing  $q$  suggesting that the system can only tunnel within a restricted subset of topological sectors. Together with the power-law scaling of open Wilson strings in this phase, this behavior supports the interpretation in terms of Coulombic states with emergent gapless photons.

the non-decodable phase it saturates to an  $\mathcal{O}(1)$  value. This equates decodability with the presence of topological order in the METTS states, and non-decodability with their topological triviality. In the information critical phase, we find that the amplitude for topological tunneling saturates to a constant that is independent of system size, precisely as predicted by spin wave theory. Nevertheless, this saturation value decays sharply with the charge  $q$  of the Wilson loop. As a result, at fixed decoherence strength the system can effectively tunnel only within a restricted subset of topological sectors, since the creation of large charge loops remains exponentially suppressed. This behavior provides a simple physical explanation for the fractional protection of logical information in this phase. Logical information encoded in superpositions of sectors separated by large charge differences is effectively protected, as decoherence is unable to induce tunneling between these sectors. In contrast, information stored in superpositions of logical states differing by small charges is efficiently destroyed. As the decoherence strength is increased, additional charge sectors are progressively unlocked, leading to a continuous erosion of the protected logical subspace.

To gain further insight into these states, we consider-

ing the expectation value of an open Wilson string  $\langle X_\gamma \rangle$  which creates a pair of electric charges  $\pm 1$  at its end points  $\partial\gamma$ . If the separation of the charges is taken to be large  $\gamma \gg 1$ , this expectation value serves as an order parameter for detecting the condensation of electric charges in the gauge states  $|\psi_Q\rangle$ . It is plotted in Fig. 5 under a different name, namely the Rényi-1 correlator which will be defined in the next section. In the decodable phase, we find  $\langle X_\gamma \rangle \sim e^{-\alpha|\gamma|}$  decays exponentially with the separation of the charges. On the other hand, in the non-decodable phase,  $\langle X_\gamma \rangle \sim \mathcal{O}(1)$  in the limit  $|\gamma| \rightarrow \infty$  indicating condensation of electric charges, pointing to a “Higgs phase”. In the information critical phase, the open string expectation value exhibits a power-law decay,  $\langle X_\gamma \rangle \sim |\gamma|^{-\eta(T)}$  where the exponent  $\eta(T)$  itself continuously changes with decoherence strength. This implies the presence of gapless modes which can be naturally interpreted as emergent photons, placing this regime in direct analogy with a Coulomb phase of a  $2 + 1$  dimensional  $U(1)$  gauge theory. We conclude that the states  $|\psi_Q(\mathbf{x})\rangle$  appearing in the convex decomposition of the mixed state may be viewed as gapless Coulomb states.

While this does not strictly rule out the possibility that the decohered density matrix in the information critical phase admits a decomposition as a convex mixture of genuine SRE states, we consider this scenario unlikely in light of the nonzero coherent information. We note that it would be interesting to directly probe the long-range entanglement structure of the information critical phase directly using genuine mixed state diagnostics, such as the topological entanglement negativity, and to determine whether this quantity likewise saturates to a fractional value in this regime. We leave a detailed investigation of this question for future work.

## V. DUAL STRONG-TO-WEAK SSB

Our results also immediately reveal the mixed state phase diagrams of a family of decohered spin systems which are obtained by “ungauging” the  $\mathbb{Z}_N$  Toric code via Kramers-Wannier (KW) duality. Under this duality, the flux free sector of the  $\mathbb{Z}_N$  Toric code (corresponding to  $B_p = 1$  for all  $p$ ) can be mapped to a  $\mathbb{Z}_N$  quantum spin model via the following operator dictionary

$$A_v \longleftrightarrow \bar{X}_v \\ X_{\mu=\langle v_1 \rightarrow v_2 \rangle} \longleftrightarrow \bar{Z}_{v_1}(\bar{Z}_{v_2})^\dagger \quad (60)$$

In this representation, the spins reside on the vertices, and in the  $\bar{X}$  basis, their eigenvalues directly encode the anyon charge at each vertex. Moreover, the “Bianchi identity”  $\prod_v A_v = 1$  is promoted to a global 0-form  $\mathbb{Z}_N$  symmetry  $\prod_v \bar{X}_v = 1$ , reflecting conservation of total anyon charge, whereas the Toric code ground state  $|\Psi_0\rangle$  with  $A_v = 1$  for all  $v$  is mapped to the (paramagnetic) product state  $\otimes_v |\bar{X}_v = 1\rangle$ .

We again consider only  $X$  type dephasing in the  $\mathbb{Z}_N$  Toric code. Since this noise preserves the flux free con-

straint ( $B_p = 1$ ), the KW dictionary continues to hold. In the dual spin model, this local decoherence channel acting on each link  $\langle v \rightarrow v' \rangle$  takes the form

$$\mathcal{E}_{\langle v \rightarrow v' \rangle}(\rho) = \sum_{k=0}^{N-1} p_k^z (\bar{Z}_v \bar{Z}_{v'}^\dagger)^k \rho (\bar{Z}_{v'} \bar{Z}_v^\dagger)^k. \quad (61)$$

The resulting decohered spin state can now be diagonalized in the  $\bar{X}$  basis, yielding

$$\mathcal{E}(\rho) = \sum_{\mathbf{e}} \mathcal{Z}[\mathbf{e}, 0] |\mathbf{e}\rangle \langle \mathbf{e}|, \quad (62)$$

where  $|\mathbf{e}\rangle = \otimes_v |\bar{X}_v = e_v\rangle$ .

In this dual  $\mathbb{Z}_N$  symmetric spin system, the decoherence induced phase diagram can be naturally interpreted in the language of strong-to-weak spontaneous symmetry breaking (SWSSB) [27, 66–73]. Recall that a mixed state  $\rho$  is said to possess a *strong* (or exact)  $G$  symmetry, with a unitary representation  $U : G \rightarrow \mathcal{U}(\mathcal{H})$ , if

$$U(g)\rho = e^{i\theta_g} \rho. \quad (63)$$

for all  $g \in G$ . On the other hand, it is said to possess a *weak* (or average)  $G$  symmetry if

$$U(g)\rho U(g)^\dagger = \rho. \quad (64)$$

Operationally, strong symmetry implies that every pure state appearing in an ensemble decomposition of  $\rho$  carries the same symmetry charge, whereas weak symmetry allows the ensemble to contain states with different (but individually well defined) symmetry charges. Physically, which symmetry is realized depends on whether the system effectively exchanges particles charged under the  $G$  symmetry with the environment: strong symmetry arises in a “canonical” setting where such exchange is forbidden, while weak symmetry is characteristic of a “grand canonical” setting where charge exchange is allowed.

The distinction between strong and weak symmetries also extends to quantum channels. In particular, let  $\mathcal{E}(\cdot) = \sum_i \mathcal{K}_i(\cdot) \mathcal{K}_i^\dagger$  denote a generic quantum channel with Kraus operators  $\mathcal{K}_i$ . The channel  $\mathcal{E}(\cdot)$  is said to possess a weak  $G$  symmetry if it obeys the following covariance condition for all density matrices  $\rho$

$$\mathcal{E}\left(U_g \rho U_g^\dagger\right) = U_g \mathcal{E}(\rho) U_g^\dagger. \quad (65)$$

On the other hand, we say the channel possesses a strong  $G$  symmetry if each individual Kraus operator commutes with the symmetry

$$[\mathcal{K}_i, U_g] = 0. \quad (66)$$

SWSSB occurs when a strongly symmetric quantum channel spontaneously breaks the strong symmetry of an initial state down to a weak symmetry. A particularly transparent way to understand SWSSB is to reinterpret it as an ordinary SSB transition in a doubled Hilbert

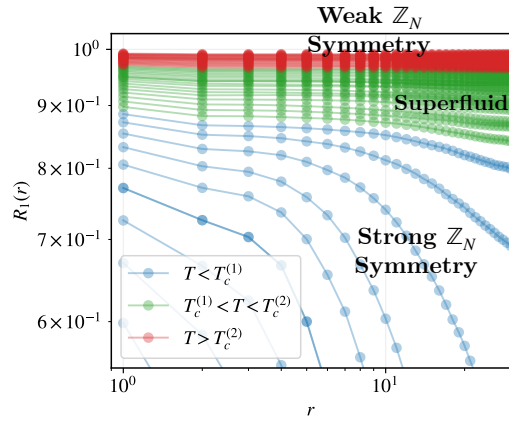


**FIG. 5. Rényi-1 Correlator.** We plot the Rényi-1 correlator in the Kramers Wannier dual of the decohered  $\mathbb{Z}_8$  Toric code for a range of decoherence temperatures, where  $r$  denotes the separation between the dual spins. We find that for  $T < T_c^{(1)}$ , corresponding to the decodable phase of the Toric code,  $R_1(r) \sim e^{-r\alpha}$  indicating the persistence of strong  $\mathbb{Z}_N$  symmetry. For  $T > T_c^{(2)}$ , corresponding to the non-decodable phase,  $R_1(r) \sim \mathcal{O}(1)$  as  $r \rightarrow \infty$  signaling SWSSB. For  $T_c^{(1)} \leq T \leq T_c^{(2)}$ , we find that  $R_1(r) \sim r^{-\eta(T)}$  exhibits an approximate power-law scaling. This points to a superfluid phase with quasi-long-range order.

space. Following Ref. [69], we consider the *canonical purification* of  $\rho$ , defined as the Choi-Jamiołkowski vectorization [106, 107] of the operator  $\sqrt{\rho} : \mathcal{H} \rightarrow \mathcal{H}$ . This yields the state  $\|\sqrt{\rho}\rangle \in \mathcal{H} \otimes \mathcal{H}^*$ , that is given by

$$\|\sqrt{\rho}\rangle = (\sqrt{\rho} \otimes 1) \sum_{\mathbf{s}} |\mathbf{s}\rangle_L |\mathbf{s}\rangle_R. \quad (67)$$

Here  $L$  denotes the original Hilbert space with orthonormal basis  $|\mathbf{s}\rangle$ , and  $R$  its charge conjugate counterpart. By construction,  $\|\sqrt{\rho}\rangle$  purifies the state  $\rho$  since

$$\rho = \text{Tr}_R \|\sqrt{\rho}\rangle \langle \sqrt{\rho}\|. \quad (68)$$

If  $\rho$  has strong  $G$  symmetry, then  $\|\sqrt{\rho}\rangle$  is invariant under  $G^L \times G^R$ , an independent  $G$  action on both copies of the Hilbert space. By contrast, if  $\rho$  only has weak  $G$  symmetry, then the purification is invariant only under the diagonal (“vector”) subgroup  $G^V \subset G^L \times G^R$ . Consequently, SWSSB in the mixed state can be viewed as a conventional SSB transition in the canonical purification, where the  $G^L \times G^R$  symmetry spontaneously breaks down to  $G^V$ . The off-diagonal (“axial”) subgroup  $G^A$  is spontaneously broken.

To sharply diagnose such a transition, we need to check if an operator in the doubled Hilbert space that is charged under the  $G^L \times G^R$  symmetry but neutral under the  $G^V$  symmetry develops long range order. Let  $\mathcal{O}_x^L (\mathcal{O}_x^R)^*$  denote such an operator. Accordingly, a natural diagnostic

of SWSSB is the following *Rényi-1 correlator* [69]

$$R_1(x-y) = \langle\langle \sqrt{\rho} | \mathcal{O}_x^L (\mathcal{O}_x^R)^* (\mathcal{O}_y^L (\mathcal{O}_y^R)^*)^\dagger | \sqrt{\rho} \rangle\rangle \\ = \text{Tr}\{ \sqrt{\rho} \mathcal{O}_x (\mathcal{O}_y)^\dagger \sqrt{\rho} \mathcal{O}_y (\mathcal{O}_x)^\dagger \} \quad (69)$$

In the limit  $r = |x-y| \rightarrow \infty$ , a nonvanishing asymptote  $R_1(r) \sim \mathcal{O}(1)$  signals spontaneous breaking of  $G^L \times G^R$  down to  $G^V$ . The correlator  $R_1$  is especially convenient because it admits a direct interpretation as an ordinary SSB correlator in the doubled Hilbert space, analogous to the more familiar Rényi-2 correlator [27]. Moreover, it directly inherits stability property which has been proved for the related *fidelity correlator* [68] which states that mixed states on opposite sides of an SWSSB transition cannot be 2-way connected by finite-depth channels that preserve the strong symmetry. For stabilizer states subject to Pauli decoherence channels, the Rényi-1 correlator and the fidelity correlator are in fact exactly equal [69].

Returning to the KW dual spin model, we note that the decoherence channel in Eq. (61) preserves the strong  $\mathbb{Z}_N$  symmetry generated by  $\prod_v \bar{X}_v$ . Furthermore, we note that the canonically purified decohered density matrix is simply given by

$$\langle\langle \sqrt{\rho} \rangle\rangle = \sum_{\mathbf{e}} \left[ \sqrt{\mathcal{Z}[\mathbf{e}, 0]} \right] |\mathbf{e}\rangle_L |-\mathbf{e}\rangle_R \quad (70)$$

To diagnose whether this state undergoes SWSSB, we compute the Rényi-1 correlator of the local operator  $\bar{Z}_x^L (\bar{Z}_x^R)^*$  in the doubled Hilbert space. This operator is clearly charged under  $\mathbb{Z}_N^L \times \mathbb{Z}_N^R$  but is neutral under the vector subgroup  $\mathbb{Z}_N^V$ . Consequently, the emergence of long-range order in this correlator signals the SWSSB in the decohered density matrix. Explicitly, we find that the Rényi-1 correlator takes the following form

$$R_1(x-y) = \sum_{\mathbf{e}} \mathcal{Z}[\mathbf{e}, 0] \sqrt{\frac{\mathcal{Z}[\mathbf{e} + \mathbf{e}_{xy}, 0]}{\mathcal{Z}[\mathbf{e}, 0]}} \quad (71)$$

where  $\mathbf{e}_{xy}$  denotes charge insertions of magnitude  $\pm 1$  at  $x$  and  $y$ . The above expression is just a disorder averaged defect-defect correlator for the classical spin model along the Nishimori line. We can compute it numerically using the same techniques laid out in Sec. III B. We depict the resulting plot for the  $\mathbb{Z}_8$  Toric code in Fig. 5.

For  $N > 4$ , we find three distinct behaviors of the defect-defect correlator  $R_1(r)$  across the phase diagram. At low  $T$ , when the Toric code is in the *decodable* phase, we find that  $R_1(r)$  decays exponentially  $R_1(r) \sim e^{-\alpha r}$  indicating the absence of long-range order in  $R_1(r)$  and the persistence of strong  $\mathbb{Z}_N^L \times \mathbb{Z}_N^R$  symmetry. Anyons remain closely confined together in this phase. On the other hand, at high  $T$ , when the Toric code is in the *non-decodable* phase, the correlator saturates to a nonzero constant,  $R_1(\gamma) \sim \mathcal{O}(1)$ , signaling the spontaneous breaking of  $\mathbb{Z}_N^L \times \mathbb{Z}_N^R$  down to the diagonal subgroup  $\mathbb{Z}_N^V$ . Although the net anyon charge always remains fixed (at zero), anyon pairs proliferate in this phase.

Interestingly, in the information critical phase, the Rényi-1 correlator exhibits a power law  $R_1(r) \sim r^{-\eta(T)}$  where the exponent  $\eta(T)$  depends on the decoherence temperature  $T$ . This behavior again arises because in this regime, the discrete  $\mathbb{Z}_N$  locking terms become RG irrelevant leading to an effective enhancement of the symmetry to a continuous  $U(1)$  group at long distances. Consequently, the infrared physics of the decohered  $\mathbb{Z}_N$  spin model in the information-critical phase closely parallels that of a decohered  $U(1)$  XY model. This effective symmetry enhancement of the broken (axial)  $\mathbb{Z}_N^A$  symmetry to a  $U(1)^A$  symmetry, places the system in a novel *superfluid phase* with quasi-long-range order. The gapless modes which are responsible for the observed power law decay of the correlator in Eq. (71) couple both copies of the Hilbert space. We can view these excitations as collective modes involving both the system and the environment. Thus, as illustrated in Fig. 1(b), the full pattern of SWSSB that we observed for the KW dual of the decohered  $\mathbb{Z}_{N>4}$  Toric code is

$$\text{Fully symmetric} \longrightarrow U(1)^A \text{ QLRO} \longrightarrow \mathbb{Z}_n^A \text{ SSB} \quad (72)$$

Finally note that the Rényi-1 correlator considered here is exactly equal to the expectation value of an open Wilson string,  $\langle X_\gamma \rangle$  evaluated in the METTS wavefunction  $|\psi_Q(1)\rangle$ . This exact correspondence provides a transparent link between the pattern of SWSSB in the dual spin model and the topological properties encoded in the METTS wavefunctions.

## VI. DECODING PROTOCOLS

We now introduce a decoding protocol for the  $\mathbb{Z}_N$  Toric code that combines a minimum-integer-cost-flow solver with a worm Monte Carlo. The coherent information analysis presented earlier provides fundamental, information-theoretic bounds on the performance achievable by any decoder. We demonstrate that the proposed decoder is optimal in the sense that its threshold coincides to very good approximation with the point at which the decohered Toric code exits the decodable phase.

The problem of formulating efficient decoding protocols for the decohered Toric code has a rich history. The decoding problem is effectively a classical post-processing task in which, given the outcomes of syndrome measurements, one seeks to identify an appropriate combination of  $X$  and  $Z$  string operators that correct the syndromes and return the system back to the codespace without incurring logical errors. More formally, the task of decoding can be described as follows. Suppose the Toric code is only subject to  $X$  type decoherence described by an arbitrary set of parameters  $\{p_k^x\}$ . This creates an incoherent mixture of  $e$  anyons. Syndromes measurements correspond to measurements of anyon charges  $\mathbf{e} = \{e_v\}$  at each vertex. The problem then reduces to finding a flow distribution  $\mathbf{k}$  which solves the divergence constraint  $(\nabla \cdot \mathbf{k})_v = e_v$  so that one can correct the syndromes by

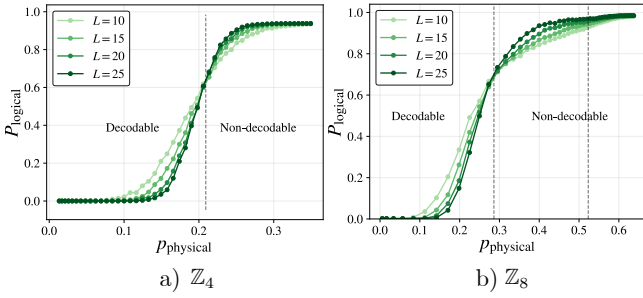


FIG. 6. **Decoding.** We present results on the performance of the proposed decoding protocol combining a minimum integer cost flow solver with a worm algorithm refinement. We plot the logical error rate,  $P_{\text{logical}}$ , as a function of the physical error rate for **a)**  $\mathbb{Z}_4$  and **b)**  $\mathbb{Z}_8$  Toric codes averaged over 1000 error realizations. In both cases we find that the error threshold appears to be very close to the decodable-fractionally decodable transition point of the decohered Toric code, implying optimality of the algorithm. In the information critical phase, the logical error rate appears to saturate to 1 in the  $L \rightarrow \infty$  limit indicating the failure of the decoder to extract the partially protected information.

applying the operator  $(X^k)^\dagger$ . However, there exist several different flow configurations which solve this constraint, all related to one another through the addition of extra divergence free flows. These distinct solutions are not equally likely; their relative probabilities depend on the noise parameters  $\{p_k^x\}$ . As a result, decoding is not merely about feasibility but is rather an optimization problem over equivalence classes of flows.

Within this framework, one can broadly distinguish between *hard-decision* and *soft-decision* decoding strategies. Hard-decision decoders select a single flow configuration to cancel the measured syndromes. Such decoders succeed provided the chosen configuration does not introduce spurious noncontractible loops that implement a logical error. For the  $\mathbb{Z}_2$  Toric code, Minimum Weight Perfect Matching (MWPM) algorithm [21], which has an efficient implementation based on Edmonds' blossom algorithm [108], serves as a powerful hard-decision decoder achieving a high threshold. Other prominent examples include hard-decision RG decoders [74, 75]. By contrast, soft-decision decoders are probabilistic decoders that assign likelihoods to different flow configurations and produce a distribution over all homology sectors. Prominent examples are soft-decision RG decoders [76–79].

We now formulate a new decoding protocol for the  $\mathbb{Z}_N$  Toric code that combines elements of both hard and soft decision decoders. The decoder proceeds in two stages. First, given a collection of syndrome measurements  $\{e_v\}$ , we solve a minimum integer cost flow problem to find a flow  $\mathbf{k}^{\text{mcf}}$  which solves the divergence constraint  $(\nabla \cdot \mathbf{k}^{\text{mcf}})_v = e_v$ . This can be viewed as a natural generalization of the MWPM algorithm. This algorithm requires integer conservation laws, so we temporarily lift all mod  $N$  constraints and shift the syndrome values to

the symmetric integer range  $e_v \in \{-[N/2], \dots, [N/2]\}$ . The solver then returns the minimum-cost solution  $\mathbf{k}^{\text{mcf}}$  that reproduces the syndromes, where the cost function  $\sum_\mu |k_\mu|$  penalizes the total magnitude of the flow. This step is an exact polynomial-time algorithm, but it is purely geometric: it does not incorporate the microscopic noise probabilities  $\{p_k^x\}$ . Note that optimizing over arbitrary non-convex cost functions is NP-hard.

One can markedly improve on the performance of this algorithm by carrying out a Monte Carlo sampling using the worm-algorithm with the “quenched background”  $\mathbf{k}^{\text{mcf}}$ . The worm updates generate divergence-free flows that explore different homology sectors, with Boltzmann weights determined by the physical noise probabilities  $\{p_k^x\}$ . This implements a soft-decision, maximum-likelihood refinement conditioned on the initial mcf solution, yielding a probability distribution over different homology sectors,  $P(\mathbf{a}|\mathbf{k}^{\text{mcf}})$ . Decoding is completed by selecting the most probable sector  $\mathbf{a}_*$  and applying the correction operator  $(X^{\mathbf{a}_*})^\dagger (X^{\mathbf{k}^{\text{mcf}}})^\dagger$ . The performance for this hybrid decoder is presented in Fig. 6. We track the logical error probability  $P_{\text{logical}}$  as a function of the physical error rate  $p_{\text{physical}}$ . In our noise model, the physical error rate is given by  $p_{\text{physical}} = 1 - p_0^x(T^x)$ . We find that the decoding threshold extracted from  $P_{\text{logical}}$  agrees, to good accuracy, with the critical point between the decodable and fractionally decodable regimes of the decohered Toric code, as diagnosed by the coherent information, providing strong evidence for the optimality of the decoder. However, in the information critical phase, we find that  $P_{\text{logical}}$  appears to increase with increasing  $L$  indicating that the decoder fails. It would appear that extracting the fractionally protected logical information that persists in the information critical phase requires a fundamentally different class of decoders.

## VII. DISCUSSION

In this work, we have extended the landscape of mixed state phases by introducing an information critical phase: extended regions of phase space in which the Markov length diverges while the conventional correlation length remains finite. Such a phase is realized in decohered  $\mathbb{Z}_N$  Toric codes for  $N > 4$  subject to decoherence. In this regime, the Toric code functions as a fractional quantum memory, preserving a finite fraction of logical information. We further showed that the decohered state in this phase admits an interpretation as a convex ensemble of Coulombic pure states. In the ungauged, Kramers-Wannier dual of the  $\mathbb{Z}_N$  Toric code, the information critical phase corresponds to a superfluid-like phase with gapless modes arising from coherent collective fluctuations of both the system and the environment. From the perspective of strong-to-weak SSB, the information critical phase arises due to an effective enhancement of the broken axial  $\mathbb{Z}_N$  symmetry to a continuous  $U(1)$  symmetry. Finally, we have introduced a new decoding algorithm for the cor-

rupted  $\mathbb{Z}_N$  Toric code, which combines a minimum integer cost flow solver with a worm-algorithm refinement. We showed that this decoder is optimal in the sense that its threshold coincides with the fundamental decodability threshold set by the coherent information.

Several directions for future work follow naturally from our results. Firstly, while the coherent information remains finite in the information critical phase, we've found that the decoder that is optimal in the perfectly decodable phase appears to fail in this regime. This indicates that the logical degrees of freedom which remain protected under decoherence are no longer faithfully represented by the original encoding-decoding process. Identifying an appropriate encoding that targets this fractional protected subspace, and developing a faithful decoding protocol for the information critical phase, therefore constitute important directions for future work.

A second, and perhaps deeper, direction is to clarify how one should *characterize* an information critical phase. Conventional criticality admits an effective CFT description and is organized by a set of universal data such as scaling dimensions and operator product coefficients. By contrast, in a particular family of examples, we showed that criticality is realized through a *disordered ensemble* of critical states, so different observables can be governed by different effective scaling exponents. Indeed, disordered critical systems are known to exhibit an infinite family of scaling dimensions depending on the observable and on the moment being probed [109, 110]. Developing an analogous set of universal descriptors for information criticality, both from an information-theoretic and a field-theoretic view, remains an important open problem. Along the same line, it would also be interesting to understand the information critical phase using recently proposed mixed-state bootstrap framework [58]. For example, a sharper characterization of the scale-invariant behavior of the conditional mutual information in this phase would be valuable.

Furthermore, our analysis was restricted to charge-

conjugation-symmetric dephasing channels. It is therefore natural to ask whether the information-critical phase survives once this symmetry is broken. In the corresponding statistical-mechanical description, such symmetry breaking maps on to a *chiral* clock model [111, 112], which comes with a sign problem and lies beyond the classical Monte carlo techniques exploited here. Establishing the stability of the information critical phase in this more generic setting would provide a stringent test of the robustness of the phase and help identify which aspects are truly universal.

Finally, our study of the dual  $\mathbb{Z}_N$  SWSSB transition indicates that, under a strongly  $\mathbb{Z}_N$  symmetric Lindbladian evolution, there exists a time range where the system may exhibit *emergent*  $U(1)$  symmetry. As the presence of strong  $U(1)$  symmetry in the Lindbladian dynamics is related to the presence of diffusive behaviors [66, 113], it would be interesting to study whether the presence of emergent continuous symmetry can give rise to novel diffusive behaviors in intermediate timescales.

*Notes added:* While preparing this manuscript, we became aware of an independent work on decohered  $U(1)$  symmetry enriched topological codes, which implements minimum integer flow alongside worm decoders [114].

## ACKNOWLEDGMENTS

We thank Tai-Hsuan Yang, Andreas Ludwig, and Ehud Altman for several fruitful discussions. In particular, we thank Zack Weinstein for directing us to the Worm algorithm that significantly expedited the numerical simulation. The work is supported by the faculty startup grant at the University of Illinois, Urbana-Champaign and the IBM-Illinois Discovery Accelerator Institute. Additionally, JYL and AV acknowledge support from KIAS through the Quantum Universe Center scholar program.

---

- [1] P. W. Shor, Scheme for reducing decoherence in quantum computer memory, *Phys. Rev. A* **52**, R2493 (1995).
- [2] A. R. Calderbank and P. W. Shor, Good quantum error-correcting codes exist, *Physical Review A* **54**, 1098–1105 (1996).
- [3] A. M. Steane, Error correcting codes in quantum theory, *Phys. Rev. Lett.* **77**, 793 (1996).
- [4] R. Laflamme, C. Miquel, J. P. Paz, and W. H. Zurek, Perfect quantum error correcting code, *Phys. Rev. Lett.* **77**, 198 (1996).
- [5] D. Gottesman, *An introduction to quantum error correction and fault-tolerant quantum computation* (2009), arXiv:0904.2557 [quant-ph].
- [6] M. H. Freedman, A. Kitaev, M. J. Larsen, and Z. Wang, *Topological quantum computation* (2002), arXiv:quant-ph/0101025 [quant-ph].
- [7] A. Kitaev, Fault-tolerant quantum computation by anyons, *Annals of Physics* **303**, 2–30 (2003).
- [8] S. B. Bravyi and A. Y. Kitaev, *Quantum codes on a lattice with boundary* (1998), arXiv:quant-ph/9811052 [quant-ph].
- [9] B. M. Terhal, Quantum error correction for quantum memories, *Reviews of Modern Physics* **87**, 307–346 (2015).
- [10] C. Nayak, S. H. Simon, A. Stern, M. Freedman, and S. Das Sarma, Non-abelian anyons and topological quantum computation, *Reviews of Modern Physics* **80**, 1083–1159 (2008).
- [11] H. Bombin and M. A. Martin-Delgado, Topological quantum distillation, *Physical Review Letters* **97**, 10.1103/physrevlett.97.180501 (2006).
- [12] S. Bravyi, Subsystem codes with spatially local generators, *Physical Review A* **83**, 10.1103/phys

rev.83.012320 (2011).

[13] J. Haah, Local stabilizer codes in three dimensions without string logical operators, *Physical Review A* **83**, 10.1103/physreva.83.042330 (2011).

[14] H. Bombin, Topological subsystem codes, *Phys. Rev. A* **81**, 032301 (2010).

[15] X. G. WEN, Topological orders in rigid states, *International Journal of Modern Physics B* **04**, 239 (1990), <https://doi.org/10.1142/S0217979290000139>.

[16] M. A. Levin and X.-G. Wen, String-net condensation: A physical mechanism for topological phases, *Physical Review B* **71**, 10.1103/physrevb.71.045110 (2005).

[17] M. Levin and X.-G. Wen, Detecting topological order in a ground state wave function, *Physical Review Letters* **96**, 10.1103/physrevlett.96.110405 (2006).

[18] A. Kitaev and J. Preskill, Topological entanglement entropy, *Phys. Rev. Lett.* **96**, 110404 (2006).

[19] X.-G. Wen, *Quantum Field Theory of Many-Body Systems: From the Origin of Sound to an Origin of Light and Electrons* (Oxford University Press, 2007).

[20] X.-G. Wen, Colloquium: Zoo of quantum-topological phases of matter, *Rev. Mod. Phys.* **89**, 041004 (2017).

[21] E. Dennis, A. Kitaev, A. Landahl, and J. Preskill, Topological quantum memory, *Journal of Mathematical Physics* **43**, 4452–4505 (2002).

[22] C. Wang, J. Harrington, and J. Preskill, Confinement-higgs transition in a disordered gauge theory and the accuracy threshold for quantum memory, *Annals of Physics* **303**, 31–58 (2003).

[23] H. G. Katzgraber, H. Bombin, and M. A. Martin-Delgado, Error threshold for color codes and random three-body ising models, *Physical Review Letters* **103**, 10.1103/physrevlett.103.090501 (2009).

[24] H. Bombin, R. S. Andrist, M. Ohzeki, H. G. Katzgraber, and M. A. Martin-Delgado, Strong resilience of topological codes to depolarization, *Physical Review X* **2**, 10.1103/physrevx.2.021004 (2012).

[25] A. Kubica, M. E. Beverland, F. Brandão, J. Preskill, and K. M. Svore, Three-dimensional color code thresholds via statistical-mechanical mapping, *Physical Review Letters* **120**, 10.1103/physrevlett.120.180501 (2018).

[26] R. Fan, Y. Bao, E. Altman, and A. Vishwanath, Diagnostics of mixed-state topological order and breakdown of quantum memory, *PRX Quantum* **5**, 020343 (2024).

[27] J. Y. Lee, C.-M. Jian, and C. Xu, Quantum criticality under decoherence or weak measurement, *PRX Quantum* **4**, 030317 (2023).

[28] J. Y. Lee, Exact calculations of coherent information for toric codes under decoherence: Identifying the fundamental error threshold, *Physical Review Letters* **134**, 10.1103/hlfh-86yz (2025).

[29] Y. Zhao and D. E. Liu, Extracting error thresholds through the framework of approximate quantum error correction condition, *Phys. Rev. Res.* **6**, 043258 (2024).

[30] R. Niwa and J. Y. Lee, Coherent information for calderbank-shor-steane codes under decoherence, *Phys. Rev. A* **111**, 032402 (2025).

[31] A. Lyons, Understanding stabilizer codes under local decoherence through a general statistical mechanics mapping (2024), [arXiv:2403.03955 \[quant-ph\]](https://arxiv.org/abs/2403.03955).

[32] Y. Zhao and D. E. Liu, Extracting error thresholds through the framework of approximate quantum error correction condition, *Phys. Rev. Res.* **6**, 043258 (2024).

[33] K. Su, Z. Yang, and C.-M. Jian, Tapestry of dualities in decohered quantum error correction codes, *Physical Review B* **110**, 10.1103/physrevb.110.085158 (2024).

[34] M. B. Hastings and X.-G. Wen, Quasiadiabatic continuation of quantum states: The stability of topological ground-state degeneracy and emergent gauge invariance, *Phys. Rev. B* **72**, 045141 (2005).

[35] X. Chen, Z.-C. Gu, and X.-G. Wen, Local unitary transformation, long-range quantum entanglement, wave function renormalization, and topological order, *Phys. Rev. B* **82**, 155138 (2010).

[36] N. Schuch, D. Pérez-García, and I. Cirac, Classifying quantum phases using matrix product states and projected entangled pair states, *Phys. Rev. B* **84**, 165139 (2011).

[37] X. Chen, Z.-C. Gu, and X.-G. Wen, Complete classification of one-dimensional gapped quantum phases in interacting spin systems, *Phys. Rev. B* **84**, 235128 (2011).

[38] M. B. Hastings, Topological order at nonzero temperature, *Phys. Rev. Lett.* **107**, 210501 (2011).

[39] Y. A. Lee and G. Vidal, Entanglement negativity and topological order, *Phys. Rev. A* **88**, 042318 (2013).

[40] C. Castelnovo, Negativity and topological order in the toric code, *Phys. Rev. A* **88**, 042319 (2013).

[41] T.-C. Lu, T. H. Hsieh, and T. Grover, Detecting topological order at finite temperature using entanglement negativity, *Phys. Rev. Lett.* **125**, 116801 (2020).

[42] O. Hart and C. Castelnovo, Entanglement negativity and sudden death in the toric code at finite temperature, *Phys. Rev. B* **97**, 144410 (2018).

[43] T.-T. Wang, M. Song, Z. Y. Meng, and T. Grover, Analog of topological entanglement entropy for mixed states, *PRX Quantum* **6**, 010358 (2025).

[44] T.-C. Lu and S. Vijay, Characterizing long-range entanglement in a mixed state through an emergent order on the entangling surface (2022), [arXiv:2201.07792 \[cond-mat.str-el\]](https://arxiv.org/abs/2201.07792).

[45] A. Coser and D. Pérez-García, Classification of phases for mixed states via fast dissipative evolution, *Quantum* **3**, 174 (2019).

[46] R. Sohal and A. Prem, Noisy approach to intrinsically mixed-state topological order, *PRX Quantum* **6**, 010313 (2025).

[47] Y. Bao, R. Fan, A. Vishwanath, and E. Altman, Mixed-state topological order and the errorfield double formulation of decoherence-induced transitions (2023), [arXiv:2301.05687 \[quant-ph\]](https://arxiv.org/abs/2301.05687).

[48] S. Sang and T. H. Hsieh, Stability of mixed-state quantum phases via finite markov length (2024), [arXiv:2404.07251 \[quant-ph\]](https://arxiv.org/abs/2404.07251).

[49] Z. Wang, Z. Wu, and Z. Wang, Intrinsic mixed-state topological order, *PRX Quantum* **6**, 010314 (2025).

[50] T. D. Ellison and M. Cheng, Toward a classification of mixed-state topological orders in two dimensions, *PRX Quantum* **6**, 10.1103/prxquantum.6.010315 (2025).

[51] S. Sang, Y. Zou, and T. H. Hsieh, Mixed-state quantum phases: Renormalization and quantum error correction, *Phys. Rev. X* **14**, 031044 (2024).

[52] Z. Wang and L. Li, Anomaly in open quantum systems and its implications on mixed-state quantum phases (2024), [arXiv:2403.14533 \[quant-ph\]](https://arxiv.org/abs/2403.14533).

[53] Y.-H. Chen and T. Grover, Separability transitions in topological states induced by local decoherence, *Physical Review Letters* **132**, 10.1103/physrevlett.132.170602

(2024).

[54] Y.-H. Chen and T. Grover, Symmetry-enforced many-body separability transitions, *PRX Quantum* **5**, 10.1103/prxquantum.5.030310 (2024).

[55] Y.-H. Chen and T. Grover, Unconventional topological mixed-state transition and critical phase induced by self-dual coherent errors, *Phys. Rev. B* **110**, 125152 (2024).

[56] S. Sang, L. A. Lessa, R. S. K. Mong, T. Grover, C. Wang, and T. H. Hsieh, Mixed-state phases from local reversibility (2025), arXiv:2507.02292 [quant-ph].

[57] J. Lloyd, D. A. Abanin, and S. Gopalakrishnan, Diverging conditional correlation lengths in the approach to high temperature (2025), arXiv:2508.02567 [quant-ph].

[58] T.-H. Yang, B. Shi, and J. Y. Lee, Topological mixed states: Axiomatic approaches and phases of matter (2025), arXiv:2506.04221 [cond-mat.str-el].

[59] J. V. José, L. P. Kadanoff, S. Kirkpatrick, and D. R. Nelson, Renormalization, vortices, and symmetry-breaking perturbations in the two-dimensional planar model, *Phys. Rev. B* **16**, 1217 (1977).

[60] S. Elitzur, R. B. Pearson, and J. Shigemitsu, Phase structure of discrete abelian spin and gauge systems, *Phys. Rev. D* **19**, 3698 (1979).

[61] J. L. Cardy, General discrete planar models in two dimensions: Duality properties and phase diagrams, *Journal of Physics A: Mathematical and General* **13**, 1507 (1980).

[62] V. A. Fateev and A. B. Zamolodchikov, Parafermionic Currents in the Two-Dimensional Conformal Quantum Field Theory and Selfdual Critical Points in  $Z(n)$  Invariant Statistical Systems, *Sov. Phys. JETP* **62**, 215 (1985).

[63] T. Sasamoto and H. Nishimori, Phase structure of the random  $zq$  models in 2d, *Progress of Theoretical Physics Supplement* **157**, 82 (2005).

[64] S. Yotsuyanagi, Y. Suemitsu, and Y. Ozeki, Effects of discreteness on gauge glass models in two and three dimensions, *Phys. Rev. E* **79**, 041138 (2009).

[65] S. R. White, Minimally entangled typical quantum states at finite temperature, *Phys. Rev. Lett.* **102**, 190601 (2009).

[66] O. Ogunnaike, J. Feldmeier, and J. Y. Lee, Unifying emergent hydrodynamics and lindbladian low-energy spectra across symmetries, constraints, and long-range interactions, *Phys. Rev. Lett.* **131**, 220403 (2023).

[67] P. Sala, S. Gopalakrishnan, M. Oshikawa, and Y. You, Spontaneous strong symmetry breaking in open systems: Purification perspective, *Phys. Rev. B* **110**, 155150 (2024).

[68] L. A. Lessa, R. Ma, J.-H. Zhang, Z. Bi, M. Cheng, and C. Wang, Strong-to-weak spontaneous symmetry breaking in mixed quantum states, *PRX Quantum* **6**, 010344 (2025).

[69] Z. Weinstein, Efficient detection of strong-to-weak spontaneous symmetry breaking via the rényi-1 correlator, *Phys. Rev. Lett.* **134**, 150405 (2025).

[70] X. Huang, M. Qi, J.-H. Zhang, and A. Lucas, Hydrodynamics as the effective field theory of strong-to-weak spontaneous symmetry breaking, *Phys. Rev. B* **111**, 125147 (2025).

[71] J. Kim, E. Altman, and J. Y. Lee, Error threshold of syk codes from strong-to-weak parity symmetry breaking (2024), arXiv:2410.24225 [quant-ph].

[72] Z. Liu, L. Chen, Y. Zhang, S. Zhou, and P. Zhang, Diagnosing strong-to-weak symmetry breaking via wightman correlators (2024), arXiv:2410.09327 [quant-ph].

[73] C. Zhang, Y. Xu, J.-H. Zhang, C. Xu, Z. Bi, and Z.-X. Luo, Strong-to-weak spontaneous breaking of 1-form symmetry and intrinsically mixed topological order, *Phys. Rev. B* **111**, 115137 (2025).

[74] S. Bravyi and J. Haah, Quantum self-correction in the 3d cubic code model, *Physical Review Letters* **111**, 10.1103/physrevlett.111.200501 (2013).

[75] H. Anwar, B. J. Brown, E. T. Campbell, and D. E. Browne, Fast decoders for qudit topological codes, *New Journal of Physics* **16**, 063038 (2014).

[76] G. Duclos-Cianci and D. Poulin, Fast decoders for topological quantum codes, *Phys. Rev. Lett.* **104**, 050504 (2010).

[77] G. Duclos-Cianci and D. Poulin, A renormalization group decoding algorithm for topological quantum codes (2010), arXiv:1006.1362 [quant-ph].

[78] G. Duclos-Cianci and D. Poulin, Kitaev's  $F_d$ -code threshold estimates, *Phys. Rev. A* **87**, 062338 (2013).

[79] F. H. E. Watson, H. Anwar, and D. E. Browne, Fast fault-tolerant decoder for qubit and qudit surface codes, *Physical Review A* **92**, 10.1103/physreva.92.032309 (2015).

[80] S. Lloyd, Capacity of the noisy quantum channel, *Phys. Rev. A* **55**, 1613 (1997).

[81] P. W. Shor, Capacities of quantum channels and how to find them, *Mathematical Programming* **97**, 311–335 (2003).

[82] I. Devetak, The private classical capacity and quantum capacity of a quantum channel (2004), arXiv:quant-ph/0304127 [quant-ph].

[83] M. A. Nielsen and I. L. Chuang, *Quantum Computation and Quantum Information: 10th Anniversary Edition* (Cambridge University Press, 2010).

[84] Proceedings of the Royal Society of London. Series A: Mathematical, Physical and Engineering Sciences **452**, 2551–2577 (1996).

[85] P. Hayden, R. Jozsa, D. Petz, and A. Winter, Structure of states which satisfy strong subadditivity of quantum entropy with equality, *Communications in Mathematical Physics* **246**, 359–374 (2004).

[86] O. Fawzi and R. Renner, Quantum conditional mutual information and approximate markov chains, *Communications in Mathematical Physics* **340**, 575–611 (2015).

[87] H. Nishimori, *Statistical physics of spin glasses and information processing: an introduction*, 111 (Clarendon Press, 2001).

[88] Y. Ozeki and H. Nishimori, Phase diagram of gauge glasses, *Journal of Physics A: Mathematical and General* **26**, 3399 (1993).

[89] M. S. S. Challa and D. P. Landau, Critical behavior of the six-state clock model in two dimensions, *Phys. Rev. B* **33**, 437 (1986).

[90] S. Chatterjee, S. Puri, and R. Paul, Ordering kinetics in the  $q$ -state clock model: Scaling properties and growth laws, *Phys. Rev. E* **98**, 032109 (2018).

[91] G. Li, K. H. Pai, and Z.-C. Gu, Tensor-network renormalization approach to the  $q$ -state clock model, *Phys. Rev. Res.* **4**, 023159 (2022).

[92] E. Domany, D. Mukamel, and A. Schwimmer, Phase diagram of the  $z(5)$  model on a square lattice, *Journal of Physics A: Mathematical and General* **13**, L311 (1980).

[93] H. Ueda, K. Okunishi, K. Harada, R. Krejmár, A. Gendiar, S. Yunoki, and T. Nishino, Finite- $m$  scaling analysis of berezinskii-kosterlitz-thouless phase transitions and entanglement spectrum for the six-state clock model, *Phys. Rev. E* **101**, 062111 (2020).

[94] S. Chatterjee, S. Sutradhar, S. Puri, and R. Paul, Ordering kinetics in a  $q$ -state random-bond clock model: Role of vortices and interfaces, *Phys. Rev. E* **101**, 032128 (2020).

[95] C. Mudry and X.-G. Wen, Does quasi-long-range order in the two-dimensional xy model really survive weak random phase fluctuations?, *Nuclear Physics B* **549**, 613 (1999).

[96] A. Vijay and J. Y. Lee, Holographically emergent gauge theory in symmetric quantum circuits (2025), arXiv:2511.21685 [quant-ph].

[97] N. Prokof'ev and B. Svistunov, Worm algorithms for classical statistical models, *Phys. Rev. Lett.* **87**, 160601 (2001).

[98] N. Prokof'ev, B. Svistunov, and I. Tupitsyn, “worm” algorithm in quantum monte carlo simulations, *Physics Letters A* **238**, 253 (1998).

[99] W. Xu, Y. Sun, J.-P. Lv, and Y. Deng, High-precision monte carlo study of several models in the three-dimensional u(1) universality class, *Phys. Rev. B* **100**, 064525 (2019).

[100] H. Nishimori, Conjecture on the exact transition point of the random ising ferromagnet, *Journal of Physics C: Solid State Physics* **12**, L905 (1979).

[101] K. Takeda and H. Nishimori, Duality of the random model and the quantum toric code, *Journal of the Physical Society of Japan* **74**, 115 (2005).

[102] J.-M. Maillard, K. Nemoto, and H. Nishimori, Symmetry, complexity and multicritical point of the two-dimensional spin glass, *Journal of Physics A: Mathematical and General* **36**, 9799 (2003).

[103] H. Nishimori, Duality in finite-dimensional spin glasses, *Journal of Statistical Physics* **126**, 977–986 (2006).

[104] H. Nishimori and K. Nemoto, Duality and multicritical point of two-dimensional spin glasses, *Journal of the Physical Society of Japan* **71**, 1198–1199 (2002).

[105] M. Ohzeki and H. Nishimori, Analytical evidence for the absence of spin glass transition on self-dual lattices, *Journal of Physics A: Mathematical and Theoretical* **42**, 332001 (2009).

[106] M.-D. Choi, Completely positive linear maps on complex matrices, *Linear Algebra and its Applications* **10**, 285 (1975).

[107] A. Jamiołkowski, Linear transformations which preserve trace and positive semidefiniteness of operators, *Reports on Mathematical Physics* **3**, 275 (1972).

[108] J. Edmonds, Paths, trees, and flowers, *Canadian Journal of Mathematics* **17**, 449–467 (1965).

[109] A. W. Ludwig and J. L. Cardy, Perturbative evaluation of the conformal anomaly at new critical points with applications to random systems, *Nuclear Physics B* **285**, 687 (1987).

[110] A. W. Ludwig, Infinite hierarchies of exponents in a diluted ferromagnet and their interpretation, *Nuclear Physics B* **330**, 639 (1990).

[111] S. Whitsitt, R. Samajdar, and S. Sachdev, Quantum field theory for the chiral clock transition in one spatial dimension, *Physical Review B* **98**, 10.1103/physrevb.98.205118 (2018).

[112] R. Samajdar, S. Choi, H. Pichler, M. D. Lukin, and S. Sachdev, Numerical study of the chiral quantum phase transition in one spatial dimension, *Physical Review A* **98**, 10.1103/physreva.98.023614 (2018).

[113] S. Moudgalya and O. I. Motrunich, Symmetries as ground states of local superoperators: Hydrodynamic implications, *PRX Quantum* **5**, 040330 (2024).

[114] V. Temkin, Z. Weinstein, R. Fan, D. Podolsky, and E. Altman, To appear (2025).

[115] W. Donnelly, Decomposition of entanglement entropy in lattice gauge theory, *Physical Review D* **85**, 10.1103/physrevd.85.085004 (2012).

[116] W. Donnelly, Entanglement entropy and nonabelian gauge symmetry, *Classical and Quantum Gravity* **31**, 214003 (2014).

## Appendix A: Diagonalization of decohered density matrices

In this section, we fill in the missing details on analytic diagonalization of decohered density matrices.

### 1. Diagonalization of $\mathcal{E}(\rho_Q)$

Let us denote

$$\rho_{\mathbf{e};\mathbf{m}}^{\mathbf{a},\mathbf{b}} = |\mathbf{e}, \mathbf{m}, \mathbf{a}\rangle\langle\mathbf{e}, \mathbf{m}, \mathbf{b}| \quad (A1)$$

Since  $\mathcal{E}(\rho_Q)$  commutes with all the stabilizer operators, we may expand it as follows

$$\mathcal{E}(\rho_Q) = \sum_{\mathbf{e};\mathbf{m}} \text{Tr}\{\mathcal{E}(\rho_Q)\rho_{\mathbf{e};\mathbf{m}}^{\mathbf{b},\mathbf{a}}\} \rho_{\mathbf{e};\mathbf{m}}^{\mathbf{a},\mathbf{b}} \quad (A2)$$

Diagonalization now effectively reduces to evaluating the trace  $\text{Tr}\{\mathcal{E}(\rho_Q)\rho_{\mathbf{e}_v;\mathbf{m}_p}^{\mathbf{a},\mathbf{b}}\}$ . First we write

$$\mathcal{E}(\rho_Q) = \left( \prod_{\mu} \mathcal{E}_{\mu}^x \circ \prod_{\mu} \mathcal{E}_{\mu}^z \right) (\rho_Q) \quad (A3)$$

$$= \sum_{\{\mathbf{k}^x, \mathbf{k}^z\}} \left( \prod_{\mu} p_{k_{\mu}^x}^x p_{k_{\mu}^z}^z \right) \times \\ Z^{\mathbf{k}^z} X^{\mathbf{k}^x} \rho_Q (X^{\dagger})^{\mathbf{k}^x} (Z^{\dagger})^{\mathbf{k}^z} \quad (A4)$$

Here we sum over all possible configurations  $\{\mathbf{k}^x, \mathbf{k}^z\}$  and we've defined

$$X^{\mathbf{k}^x} = \prod_{\mu} X_{\mu}^{k_{\mu}^x}, \quad Z^{\mathbf{k}^z} = \prod_{\mu} Z_{\mu}^{k_{\mu}^z} \quad (A5)$$

Substituting the initial density matrix  $\rho_Q = \frac{1}{N^2} \sum_{\mathbf{c}} X^{\mathbf{c}} |\Psi_0\rangle\langle\Psi_0| (X^{\mathbf{c}})^{\dagger}$ , into  $\text{Tr}\{\mathcal{E}(\rho_Q)\rho_{\mathbf{e}_v;\mathbf{m}_p}^{\mathbf{a},\mathbf{b}}\}$  yields the expression

$$\text{Tr}\{\mathcal{E}(\rho_Q)\rho_{\mathbf{e};\mathbf{m}}^{\mathbf{a},\mathbf{b}}\} = \frac{1}{N^2} \sum_{\mathbf{c}} \sum_{\{\mathbf{k}^x, \mathbf{k}^z\}} \left( \prod_{\mu} p_{k_{\mu}^x}^x p_{k_{\mu}^z}^z \right) \\ \times \delta_{\mathbf{ab}} |\langle \mathbf{e}; \mathbf{m}; \mathbf{a} | Z^{\mathbf{k}^z} X^{\mathbf{k}^x} X^{\mathbf{c}} | \Psi_0 \rangle|^2 \quad (A6)$$

The matrix element  $|\langle \mathbf{e}; \mathbf{m}; \mathbf{a} | Z^{\mathbf{k}^z} X^{\mathbf{k}^x} X^{\mathbf{c}} | \Psi_0 \rangle|$  vanishes unless open Wilson strings in  $X^{\mathbf{k}^x}$  create charges  $e_v$  at their ends, i.e.  $(\nabla \cdot \mathbf{k}^x)_v = e_v \bmod N$ , and open 't Hooft strings in  $Z^{\mathbf{k}^z}$  create fluxes  $m_p$  at their ends, i.e.  $(\nabla \times \mathbf{k}^z)_p = m_p \bmod N$ . Furthermore, the state  $X^{\mathbf{k}^x} X^{\mathbf{c}} | \Psi_0 \rangle$  must be an eigenstate of  $Z_{\hat{\mathcal{C}}_2}$  and  $Z_{\hat{\mathcal{C}}_1}$  with eigenvalues  $a_1$  and  $a_2$  respectively. Equivalently, we must have  $\hat{\mathcal{C}}(\mathbf{k}^x) = \mathbf{a} - \mathbf{c}$ . If these conditions are satisfied, the absolute value of the matrix element equals 1 and if they're not satisfied, the matrix element vanishes. Thus, the trace term reduces to

$$\text{Tr}\{\mathcal{E}(\rho_Q)\rho_{\mathbf{e};\mathbf{m}}^{\mathbf{a},\mathbf{b}}\} = \frac{1}{N^2} \sum_{\mathbf{c}} \sum_{\substack{\mathbf{k}^z \\ (\nabla \times \mathbf{k}^z)_p = m_p}} \prod_{\mu} p_{k_{\mu}^z}^z \\ \sum_{\substack{\mathbf{k}^x \\ (\nabla \cdot \mathbf{k}^x)_v = e_v, \hat{\mathcal{C}}(\mathbf{k}^x) = \mathbf{a} - \mathbf{c}}} \prod_{\mu} p_{k_{\mu}^x}^x \quad (\text{A7})$$

The sum over  $\mathbf{c}$  effectively removes the  $\hat{\mathcal{C}}(\mathbf{k}^x) = \mathbf{a} - \mathbf{c}$  constraint. If we now define  $\mathcal{Z}[\mathbf{e}, \mathbf{a}]$  and  $\mathcal{Z}[\mathbf{m}, \mathbf{b}]$  as follows

$$\mathcal{Z}[\mathbf{e}, \mathbf{a}] = \sum_{\substack{\mathbf{k}^x \\ (\nabla \cdot \mathbf{k}^x)_v = e_v, \hat{\mathcal{C}}(\mathbf{k}^x) = \mathbf{a}}} \prod_{\mu} p_{k_{\mu}^x}^x \quad (\text{A8})$$

$$\mathcal{Z}[\mathbf{m}, \mathbf{b}] = \sum_{\substack{\mathbf{k}^z \\ (\nabla \times \mathbf{k}^z)_p = m_p, \hat{\mathcal{C}}(\mathbf{k}^z) = \mathbf{b}}} \prod_{\mu} p_{k_{\mu}^z}^z \quad (\text{A9})$$

then the trace term can be written compactly as

$$\text{Tr}\{\mathcal{E}(\rho_Q)\rho_{\mathbf{e};\mathbf{m}}^{\mathbf{a},\mathbf{b}}\} = \frac{1}{N^2} \mathcal{Z}[\mathbf{e}] \mathcal{Z}[\mathbf{m}] \quad (\text{A10})$$

where  $\mathcal{Z}[\mathbf{e}] = \sum_{\mathbf{a}} \mathcal{Z}[\mathbf{e}, \mathbf{a}]$  and  $\mathcal{Z}[\mathbf{m}] = \sum_{\mathbf{a}} \mathcal{Z}[\mathbf{m}, \mathbf{a}]$ . Thus, we're left with the following final expression for the de-cohered Toric code density matrix

$$\mathcal{E}(\rho_Q) = \sum_{\substack{\mathbf{e};\mathbf{m} \\ \mathbf{a}}} \frac{1}{N^2} \mathcal{Z}[\mathbf{e}] \mathcal{Z}[\mathbf{m}] \rho_{\mathbf{e};\mathbf{m}}^{\mathbf{a},\mathbf{a}} \quad (\text{A11})$$

## 2. Diagonalization or $\mathcal{E}(\rho_{QR})$

In order to compute the coherent information, we also need to diagonalize the density matrix  $\mathcal{E}(\rho_{QR}) = \mathcal{E}(|\Psi\rangle_{QR}\langle\Psi|_{QR})$  so we do this next. Recall that

$$\rho_{QR} = \frac{1}{N^2} \sum_{\mathbf{a}\mathbf{a}'} X^{\mathbf{a}} |\psi_0\rangle\langle\psi_0| (X^{\mathbf{a}'})^{\dagger} \otimes |\mathbf{a}\rangle\langle\mathbf{a}'| \quad (\text{A12})$$

Since the channel  $\mathcal{E}(\cdot)$  only acts on the Toric code degrees of freedom, we can write

$$\mathcal{E}(\rho_{QR}) = \frac{1}{N^2} \sum_{\mathbf{a}\mathbf{a}'} \mathcal{E}\left(X^{\mathbf{a}} |\Psi_0\rangle\langle\Psi_0| (X^{\mathbf{a}'})^{\dagger}\right) \otimes |\mathbf{a}\rangle\langle\mathbf{a}'| \quad (\text{A13})$$

Again  $\mathcal{E}(X^{\mathbf{a}} |\Psi_0\rangle\langle\Psi_0| (X^{\mathbf{a}'})^{\dagger})$  commutes with all the stabilizer operators so we can expand it as before in the Hamiltonian basis

$$\begin{aligned} \mathcal{E}(X_{\mathbf{a}} |\Psi_0\rangle\langle\Psi_0| X_{\mathbf{a}'}^{\dagger}) = \\ \sum_{\substack{\mathbf{e};\mathbf{m} \\ \mathbf{b},\mathbf{c}}} \text{Tr}\left\{\mathcal{E}(X_{\mathbf{a}} |\Psi_0\rangle\langle\Psi_0| X_{\mathbf{a}'}^{\dagger}) \rho_{\mathbf{e};\mathbf{m}}^{\mathbf{b},\mathbf{c}}\right\} \rho_{\mathbf{e};\mathbf{m}}^{\mathbf{c},\mathbf{b}} \end{aligned} \quad (\text{A14})$$

Substituting the expression for the channel  $\mathcal{E}(\cdot)$  then yields

$$\begin{aligned} \text{Tr}\left\{\mathcal{E}(X_{\mathbf{a}} |\Psi_0\rangle\langle\Psi_0| X_{\mathbf{a}'}^{\dagger}) \rho_{\mathbf{e};\mathbf{m}}^{\mathbf{b},\mathbf{c}}\right\} = \sum_{\{\mathbf{k}^x, \mathbf{k}^z\}} \left( \prod_{\mu} p_{k_{\mu}^x}^x p_{k_{\mu}^z}^z \right) \\ \times \langle \mathbf{e}; \mathbf{m}; \mathbf{c} | Z^{\mathbf{k}^z} X^{\mathbf{k}^x} X^{\mathbf{a}} | \Psi_0 \rangle \\ \times \langle \Psi_0 | (X^{\mathbf{a}'})^{\dagger} (X^{\mathbf{k}^x})^{\dagger} (Z^{\mathbf{k}^z})^{\dagger} | \mathbf{e}; \mathbf{m}; \mathbf{b} \rangle \end{aligned} \quad (\text{A15})$$

Once again, these matrix elements don't vanish only if the open Wilson strings in  $X^{\mathbf{k}^x}$  create charges  $e_v$  at their ends,  $(\nabla \cdot \mathbf{k}^x)_v = e_v \bmod N$ , and the open 't Hooft strings in  $Z^{\mathbf{k}^z}$  create fluxes  $m_p$  at their ends,  $(\nabla \times \mathbf{k}^z)_p = m_p \bmod N$ . Furthermore, we must have  $\hat{\mathcal{C}}(\mathbf{k}^x) = \mathbf{c} - \mathbf{a} = \mathbf{b} - \mathbf{a}'$  otherwise the whole term vanishes. Now the main difference in this calculation is that we obtain additional phase factors from moving  $X^{\mathbf{a}}$  past  $Z^{\mathbf{k}^z}$  to turn  $|\mathbf{e}; \mathbf{m}; \mathbf{c}\rangle$  into  $|\mathbf{e}; \mathbf{m}; \mathbf{c} - \mathbf{a}\rangle$  and moving  $(X^{\mathbf{a}'})^{\dagger}$  past  $(Z^{\mathbf{k}^z})^{\dagger}$  to turn  $|\mathbf{e}; \mathbf{m}; \mathbf{b}\rangle$  into  $|\mathbf{e}; \mathbf{m}; \mathbf{b} - \mathbf{a}'\rangle \equiv |\mathbf{e}; \mathbf{m}; \mathbf{c} - \mathbf{a}\rangle$ . Suppose that  $\mathcal{C}(\mathbf{k}^z) = \mathbf{d}$ , then  $Z^{\mathbf{k}^z} X^{\mathbf{a}} = \omega^{\mathbf{d} \cdot \mathbf{a}} X^{\mathbf{a}} Z^{\mathbf{k}^z}$  and  $(X^{\mathbf{a}'})^{\dagger} (Z^{\mathbf{k}^z})^{\dagger} = \omega^{-\mathbf{d} \cdot \mathbf{a}'} (Z^{\mathbf{k}^z})^{\dagger} (X^{\mathbf{a}'})^{\dagger}$ . Thus, the net phase which arises is simply  $\omega^{\mathbf{d} \cdot (\mathbf{a} - \mathbf{a}')}$  and we obtain

$$\begin{aligned} \text{Tr}\left\{\mathcal{E}(X_{\mathbf{a}} |\Psi_0\rangle\langle\Psi_0| X_{\mathbf{a}'}^{\dagger}) \rho_{\mathbf{e};\mathbf{m}}^{\mathbf{b},\mathbf{c}}\right\} = \delta_{\mathbf{c}-\mathbf{a}, \mathbf{b}-\mathbf{a}'} \\ \times \sum_{\substack{\mathbf{k}^x \\ (\nabla \cdot \mathbf{k}^x)_v = e_v, \hat{\mathcal{C}}(\mathbf{k}^x) = \mathbf{c} - \mathbf{a}}} \prod_{\mu} p_{k_{\mu}^x}^x \\ \times \sum_{\mathbf{d}} \omega^{\mathbf{d} \cdot (\mathbf{a} - \mathbf{a}')} \sum_{\substack{\mathbf{k}^z \\ (\nabla \times \mathbf{k}^z)_p = m_p, \hat{\mathcal{C}}(\mathbf{k}^z) = \mathbf{d}}} \prod_{\mu} p_{k_{\mu}^z}^z \end{aligned} \quad (\text{A16})$$

The delta function is enforced mod  $N$ . Thus the de-cohered density matrix can be written as

$$\begin{aligned} \mathcal{E}(\rho_{QR}) = \sum_{\mathbf{a}, \mathbf{a}'} \sum_{\mathbf{g}} \sum_{\mathbf{e}; \mathbf{m}} \mathcal{Z}[\mathbf{e}, \mathbf{g}] \\ \times \sum_{\mathbf{d}} \omega^{\mathbf{d} \cdot (\mathbf{a} - \mathbf{a}')} \mathcal{Z}[\mathbf{m}, \mathbf{d}] \rho_{\mathbf{e};\mathbf{m}}^{\mathbf{a} + \mathbf{g}, \mathbf{a}' + \mathbf{g}} \otimes |\mathbf{a}\rangle\langle\mathbf{a}'| \end{aligned} \quad (\text{A17})$$

It is now convenient to introduce a new orthonormal basis of the Toric code + reference Hilbert space which is defined as follows

$$|\mathbf{e}_v; \mathbf{m}_p; \mathbf{a}, \mathbf{b}\rangle_{QR} = \sum_{\mathbf{c}} \omega^{\mathbf{b} \cdot \mathbf{c}} |\mathbf{e}_v; \mathbf{m}_p; \mathbf{a} + \mathbf{c}\rangle \otimes |\mathbf{c}\rangle \quad (\text{A18})$$

Then it is immediately clear that in terms of this basis, the density matrix is fully diagonal

$$\mathcal{E}(\rho_{QR}) = \sum_{\mathbf{a}, \mathbf{b}} \sum_{\mathbf{e}; \mathbf{m}} \mathcal{Z}[\mathbf{e}, \mathbf{a}] \mathcal{Z}[\mathbf{m}, \mathbf{b}] |\mathbf{e}; \mathbf{m}; \mathbf{a}, \mathbf{b}\rangle_{QR} \langle \mathbf{e}; \mathbf{m}; \mathbf{a}, \mathbf{b}|_{QR} \quad (\text{A19})$$

Once again, we find that the spectrum of the density matrix is precisely determined by the partition functions  $\mathcal{Z}[\mathbf{e}, \mathbf{a}]$  and  $\mathcal{Z}[\mathbf{m}, \mathbf{b}]$ .

## Appendix B: Deriving Eq. (35) for the Conditional Mutual Information

Let  $A$  denote a subregion and  $\partial A$  denote the entangling boundary.  $\partial A$  partitions the links of the lattice into those lying inside region  $A$  and those lying in the complement  $\bar{A}$ . It intersects certain vertices, and the Gauss law operators associated with these boundary vertices play a particularly important role. Such a boundary vertex has incident links belonging to both subregions. As a result, once we restrict to  $A$  or  $\bar{A}$  alone, the Gauss law at that vertex can generally appear violated from the perspective of either subregion taken in isolation. Physically, this means that a nonzero electric charge may be associated with a boundary vertex when viewed from within  $A$  or  $\bar{A}$ , but this charge cannot be attributed to either side independently. Instead, it represents a shared degree of freedom that labels distinct superselection sectors for both subregions. Gauge-invariant operators supported entirely within  $A$  (or entirely within  $\bar{A}$ ) cannot modify the charge configuration along the entangling boundary  $\partial A$ . We say the boundary electric flux degrees of freedom form the *electric center* of the bipartition algebra [115, 116].

Consequently, the ground state  $|\Psi_0\rangle$  admits a decomposition of the form:

$$|\Psi_0\rangle = \frac{1}{\sqrt{\mathcal{N}_{\partial A}}} \sum_{\text{edge modes } \mathbf{e}_{\partial A}} |\mathbf{e}_{\partial A}\rangle_A |-\mathbf{e}_{\partial A}\rangle_{\bar{A}} \quad (\text{B1})$$

where the edge modes  $\mathbf{e}_{\partial A} = \{e_v \in \partial A\}$  denote the configuration of Gauss law charges on the boundary vertices  $v \in \partial A$ . They specify the superselection sectors. Since the full system imposes a global Gauss law, the boundary charge assignments are not all independent. For a simply connected region  $A$ , the total electric charge across its boundary must vanish, namely  $\sum_{v \in \partial A} e_v = 0 \pmod{N}$ . Consequently, the number of independent boundary charge configurations is  $\mathcal{N}_{\partial A} = N^{|\partial A - 1|}$ , where  $|\partial A|$  denotes the number of boundary vertices.

Now acting with an  $X$  type dephasing channel yields the following mixed state

$$\mathcal{E}(|\Psi_0\rangle\langle\Psi_0|) = \sum_{\{\mathbf{k}^x\}} \left( \prod_{\mu} p_{k_{\mu}^x}^x \right) X^{\mathbf{k}^x} |\Psi_0\rangle\langle\Psi_0| (X^{\dagger})^{\mathbf{k}^x} \quad (\text{B2})$$

Since the unitary  $X^{\mathbf{k}^x}$  clearly factorizes across the bipartition,  $X^{\mathbf{k}^x} = X_A^{\mathbf{k}^x} \otimes X_{\bar{A}}^{\mathbf{k}^x}$ , the state  $X^{\mathbf{k}^x} |\Psi_0\rangle$  also admits a decomposition of the form

$$X^{\mathbf{k}^x} |\Psi_0\rangle = \frac{1}{\sqrt{\mathcal{N}_{\partial A}}} \times \sum_{\text{edge modes } \mathbf{e}_{\partial A}} X_A^{\mathbf{k}^x} |\mathbf{e}_{\partial A}\rangle_A X_{\bar{A}}^{\mathbf{k}^x} |-\mathbf{e}_{\partial A}\rangle_{\bar{A}} \quad (\text{B3})$$

where  $X_A^{\mathbf{k}^x} = \prod_{\mu \in A} X_{\mu}^{k_{\mu}^x}$  and  $X_{\bar{A}}^{\mathbf{k}^x} = \prod_{\mu \in \bar{A}} X_{\mu}^{k_{\mu}^x}$ . Tracing out the subregion  $\bar{A}$  then yields

$$\text{Tr}_{\bar{A}} X^{\mathbf{k}^x} |\Psi_0\rangle\langle\Psi_0| (X^{\dagger})^{\mathbf{k}^x} = \frac{1}{\mathcal{N}_{\partial A}} \sum_{\mathbf{e}_{\partial A}} X_A^{\mathbf{k}^x} |\mathbf{e}_{\partial A}\rangle\langle\mathbf{e}_{\partial A}| (X_A^{\mathbf{k}^x})^{\dagger} \quad (\text{B4})$$

The reduced density matrix  $\rho_A$  continues to commute with all charge ( $A_v$ ) and flux ( $B_p$ ) operators that are entirely contained within subregion  $A$ . Moreover, the Gauss law operators associated with vertices lying on the entangling boundary  $\partial A$ , when restricted to subregion  $A$ , also commute with  $\rho_A$ . The eigenvalues of these boundary Gauss operators label the edge-mode degrees of freedom along  $\partial A$ . Consequently, the mixed state  $\mathcal{E}(|\Psi_0\rangle\langle\Psi_0|)$  can be diagonalized in the basis  $|\mathbf{e}_A, \mathbf{e}_{\partial A}\rangle$ , where  $\mathbf{e}_A$  and  $\mathbf{e}_{\partial A}$  respectively denote bulk and boundary charge configurations within  $A$ . Repeating the same analysis as before, we find that

$$\rho_A = \sum_{\mathbf{e}_A} \sum_{\mathbf{e}_{\partial A}} \frac{\mathcal{Z}[\mathbf{e}_A]}{\mathcal{N}_{\partial A}} |\mathbf{e}_A, \mathbf{e}_{\partial A}\rangle\langle\mathbf{e}_A, \mathbf{e}_{\partial A}| \quad (\text{B5})$$

where  $\mathcal{Z}[\mathbf{e}_A] = \sum_{\mathbf{e}'_{\partial A}} \mathcal{Z}[\mathbf{e}_A, \mathbf{e}'_{\partial A}]$ . Specifically, we sum over all boundary charge configurations.

Since the reduced density matrix in equation (B5) is diagonal, the Von Neumann entropy assumes a simple form

$$S(A) = (|\partial A| - 1) \log N - \sum_{\mathbf{e}_A} \mathcal{Z}[\mathbf{e}_A] \log \mathcal{Z}[\mathbf{e}_A] \quad (\text{B6})$$

The first term is the ordinary area law + TEE piece whereas the second term is the additional contribution arising due to coupling with the environment.

Now suppose  $A$  is an annulus with an inner boundary  $\partial A_{\text{in}}$  and an outer boundary  $\partial A_{\text{out}}$ . In this case, the Toric code state  $|\Psi_0\rangle$  can be decomposed as follows

$$|\Psi_0\rangle = \frac{1}{\sqrt{\mathcal{N}_{\partial A_{\text{in}}} \mathcal{N}_{\partial A_{\text{out}}}}} \times \sum_{\mathbf{e}_{\partial A_{\text{in}}}, \mathbf{e}_{\partial A_{\text{out}}}} |-\mathbf{e}_{\partial A_{\text{in}}}\rangle |\mathbf{e}_{\partial A_{\text{in}}}, \mathbf{e}_{\partial A_{\text{out}}}\rangle_A |-\mathbf{e}_{\partial A_{\text{out}}}\rangle \quad (\text{B7})$$

where  $\mathbf{e}_{\partial A_{\text{in}}}$  denotes the edge modes on the inner boundary and  $\mathbf{e}_{\partial A_{\text{out}}}$  denotes the edge modes on the outer boundary. We have a Gauss law constraint for each edge so  $\sum_{v \in \partial A_1} e_v = \sum_{v \in \partial A_2} e_v = 0 \pmod{N}$ . Equation (B4)

still holds but now the crucial difference is that the annulus itself has non-trivial homology. The unitary  $X_A^{\mathbf{k}^x}$  may, in addition to creating the charge configurations  $\mathbf{e}_A$  and  $\mathbf{e}_{\partial A}$ , also create Wilson loops that connect the inner edge to the outer edge. States with same bulk charges but with different net flux traversing from inner edge to outer edge lie in different topological sectors, characterized by their nontrivial commutation relations with the corresponding non-contractible 't Hooft loop  $Z_{\tilde{\gamma}_{\text{ann}}}$  which winds around the annulus. If  $X_A^{\mathbf{k}^x}(c)Z_{\tilde{\gamma}_{\text{ann}}} = e^{i2\pi w/N}Z_{\tilde{\gamma}_{\text{ann}}}X_A^{\mathbf{k}^x}(c)$ , we may write

$$\rho_A = \sum_{\mathbf{e}_A, w} \sum_{\substack{\mathbf{e}_{\partial A_{\text{in}}} \\ \mathbf{e}_{\partial A_{\text{out}}}}} \frac{1}{\sqrt{\mathcal{N}_{\partial A_{\text{in}}} \mathcal{N}_{\partial A_{\text{out}}}}} \mathcal{Z}[\mathbf{e}_A, w] \times \\ |\mathbf{e}_A, \mathbf{e}_{\partial A_{\text{in}}}(w), \mathbf{e}_{\partial A_{\text{out}}}(w)\rangle \langle \mathbf{e}_A, \mathbf{e}_{\partial A_{\text{in}}}(w), \mathbf{e}_{\partial A_{\text{out}}}(w)| \quad (\text{B8})$$

where  $w$  now denotes the parity of  $\mathbf{e}_{\partial A_{\text{in}}}(w)$  and  $\mathbf{e}_{\partial A_{\text{out}}}(w)$  may now both have reversed parity due to the Wilson loops stretching from inner boundary to the outer boundary. Thus, the Von-Neumann entropy for the annulus reduces to

$$S(A) = (|\partial A| - 2) \log N - \sum_{\mathbf{e}_A, w} \mathcal{Z}[\mathbf{e}_A, w] \log \mathcal{Z}[\mathbf{e}_A, w] \quad (\text{B9})$$

The crucial distinction is the appearance of the topological number  $w$ . Note that this topological number admits a precise interpretation as the net charge contained inside the annulus. Using these formulae and applying it to the annular partitions defined in (21), we arrive at Eq. (35) for the CMI.

### Appendix C: Relative Entropy

The quantum relative entropy is the natural, non-commutative generalization of the classical Kullback-Leibler divergence. For two density matrices  $\rho$  and  $\sigma$ , it takes the form

$$D(\rho||\sigma) = \text{Tr } \rho (\ln \rho - \ln \sigma) \quad (\text{C1})$$

The relative entropy is a non-negative  $D(\rho||\sigma) \geq 0$  and non-symmetric measure of distinguishability. It vanishes if and only if  $\rho = \sigma$  and it obeys the data processing inequality which states that  $D(\mathcal{E}(\rho)||\mathcal{E}(\sigma)) \leq D(\rho||\sigma)$  for any quantum channel  $\mathcal{E}(\cdot)$ . The latter is an expression of the fact that physical operations cannot increase our ability to tell states apart.

We shall be concerned with the distinguishability of two logical states of the Toric code  $X^{\mathbf{a}}|\Psi_0\rangle$  and  $X^{\mathbf{b}}|\Psi_0\rangle$  post-decoherence.

$$F^{\mathbf{a}, \mathbf{b}} = D(\mathcal{E}(\rho_0^{\mathbf{a}})||\mathcal{E}(\rho_0^{\mathbf{b}})) \quad (\text{C2})$$

Here  $\rho_0^{\mathbf{a}} = X^{\mathbf{a}}|\Psi_0\rangle\langle\Psi_0|(X^{\mathbf{a}})^\dagger$ . In the absence of decoherence, the two logical states are orthogonal to one another,

so the relative entropy is infinite. If the relative entropy remains infinite post-decoherence (in the thermodynamic limit  $L \rightarrow \infty$ ), then the two states remain perfectly distinguishable and we can reverse the effects of decoherence via the Petz recovery channel. If, however, the relative entropy drops to a finite value in the  $L \rightarrow \infty$  limit, then at least part of the logical information has been irretrievably lost, and perfect recovery is impossible.

Consider two different logical states  $|\Psi_0\rangle$  and  $(X^{\mathbf{a}})^\dagger|\Psi_0\rangle$ . From the above analysis, it is clear that the corresponding decohered density matrices take the form

$$\mathcal{E}((X^{\mathbf{a}})^\dagger|\Psi_0\rangle\langle\Psi_0|X^{\mathbf{a}}) = \sum_{\substack{\mathbf{e}: \mathbf{m} \\ \mathbf{b}}} \mathcal{Z}[\mathbf{e}, \mathbf{b} + \mathbf{a}] \mathcal{Z}[\mathbf{m}] \rho_{\mathbf{e}: \mathbf{m}}^{\mathbf{b}, \mathbf{b}} \\ \mathcal{E}(|\Psi_0\rangle\langle\Psi_0|) = \sum_{\substack{\mathbf{e}: \mathbf{m} \\ \mathbf{b}}} \mathcal{Z}[\mathbf{e}, \mathbf{b}] \mathcal{Z}[\mathbf{m}] \rho_{\mathbf{e}: \mathbf{m}}^{\mathbf{b}, \mathbf{b}} \quad (\text{C3})$$

The relative entropy between these two states is thus given by

$$F^{\mathbf{a}, \mathbf{0}} = \sum_{\mathbf{e}, \mathbf{b}} \mathcal{Z}[\mathbf{e}, \mathbf{b}] \log \frac{\mathcal{Z}[\mathbf{e}, \mathbf{b}]}{\mathcal{Z}[\mathbf{e}, \mathbf{b} + \mathbf{a}]} = \left\langle \frac{P[\mathbf{0}; \mathbf{e}]}{P[\mathbf{a}; \mathbf{e}]} \right\rangle \quad (\text{C4})$$

This is again a Nishimori line expectation. Since  $\mathcal{Z}[\mathbf{e}, \mathbf{b}]$  is a partition function for a disordered spin model with frustrations at  $\mathbf{e}$ , the relative entropy  $F^{\mathbf{a}, \mathbf{0}}$  is just the disorder-averaged excess free energy associated with an additional  $\mathbf{a}$ -twist along the non-contractible cycles of the torus.

### Appendix D: Random Bond Clock Models

We now present some analytic calculations for the coherent information and the CMI by analyzing the partition function of the random bond  $\mathbb{Z}_N$  clock model in different phases. We exploit the key property of the Nishimori line that the disorder distribution  $P(\mathbf{J})$  is proportional to the partition function itself,  $\mathcal{Z}[\mathbf{J}]$ . For concreteness, we focus on clock-model Hamiltonians with a single nonzero coupling  $\beta_1 = \beta$  which plays the role of an inverse temperature:

$$H[\{\theta_i\}; \mathbf{k}_\mathbf{a}] = -\beta \sum_{\langle i, j \rangle} \cos \frac{2\pi(\theta_i - \theta_j - k_{ij, \mathbf{a}})}{N} \quad (\text{D1})$$

The clock model is defined on an  $L \times L$  lattice with periodic boundary conditions imposed along both directions.

#### 1. Coherent Information

We begin by analysing the coherent information subject to only  $X$  type dephasing ( $Z$  type dephasing is identical). In this case, we have

$$I^{(c)}(Q : R; \mathcal{E}) = 2 \log N - [H(\mathbf{a}|\mathbf{e})] \quad (\text{D2})$$

where  $H(\mathbf{a}|\mathbf{e})$  denotes the Shannon entropy of the conditional distributions  $P[\mathbf{a}|\mathbf{e}]$ , and  $[\dots]$  denotes a disorder average on the Nishimori line.

### a. Low Temp Limit

When  $\beta \gg 1$ , the  $\mathbb{Z}_N$  clock model lies in the ordered phase. In this regime, the partition function  $\mathcal{Z}[\mathbf{e}, \mathbf{a}]$  is dominated by minimal energy saddle point configurations. Any bond configuration that contains local frustrations  $\mathbf{e}$  necessarily produces a saddle point with strictly higher energy, leading to a partition function that is exponentially suppressed in  $\beta$ . Since the Nishimori condition implies that  $P(\mathbf{J}) \sim \mathcal{Z}[\mathbf{J}]$ , all locally frustrated bond configurations must therefore be exponentially unlikely. This is unsurprising since, in this limit, the decoherence is very weak and the probability of observing charge defects should be negligible. The same argument applies to topological frustration. Since non-zero  $\mathbf{a}$  imposes twisted boundary conditions on the Torus, the energetic cost of such topological frustrations in the ordered phase must scale with system size. This immediately implies that

$$P(\mathbf{a}|\mathbf{e}) \sim e^{-L\beta c_{\mathbf{a}}} \quad (\text{D3})$$

where  $c_{\mathbf{a}} = \sum_i \cos \frac{2\pi(a_i)}{N}$ . Thus, in this phase the conditional winding entropy scales as

$$[H(\mathbf{a}|\mathbf{e})] \sim e^{-\alpha L} \quad (\text{D4})$$

leading to  $I^{(c)}(Q : R; \mathcal{E}) = 2 \log N + \mathcal{O}(e^{-L})$ . This is the decodable phase.

### b. High Temp Phase

When  $\beta \ll 1$ , the  $\mathbb{Z}_N$  clock model lies in the disordered (high-temperature) phase. In this phase, frustrations proliferate and energetics are washed out by entropic consideration. In particular introducing topological frustration  $\mathbf{a}$  has very little effect since these domain walls are screened by vortices which proliferate in this phase. This we find that

$$P(\mathbf{a}|\mathbf{e}) \sim \frac{1}{N^2} \quad (\text{D5})$$

leading to  $I^{(c)}(Q : R; \mathcal{E}) \sim 0$ . Clearly, this is the non-decodable phase.

### c. QLRO Phase

For  $N > 4$ , the  $\mathbb{Z}_N$  clock model exhibits a quasi-long-range order (QLRO) phase. In this regime, the low-energy excitations are effectively gapless spin waves, and the infrared theory is well described by a Gaussian action. We expect the same expectation holds along the

Nishimori line where bulk disorder simply renormalizes the spin stiffness. Accordingly, we model

$$\mathcal{Z}[\mathbf{e}, \mathbf{a}] = \int \mathcal{D}\varphi e^{-H[\varphi, \mathbf{J}^{\mathbf{a}}]} \quad (\text{D6})$$

$$H[\varphi, \mathbf{J}] = \frac{\kappa}{2} \int d^2x (\nabla \varphi(x) - \mathbf{J}^{\mathbf{a}}(x))^2 \quad (\text{D7})$$

$\varphi$  is a coarse-grained phase field that is effectively non-compact in this phase (vortices are suppressed), and  $\mathbf{J}^{\mathbf{a}}$  is the coarse-grained disorder field that encodes the frustrations  $\mathbf{e} = \nabla \times \mathbf{J}^{\mathbf{a}}$ .  $\kappa$  is the effective spin stiffness.  $\mathbf{J}^{\mathbf{a}}$  also encodes the topological sector data  $\mathbf{a}$ . Interpreting  $\mathbf{E} = -\nabla \varphi$  as an electric field and  $\mathbf{J}^{\mathbf{a}}$  is a polarization field, the problem maps onto a two-dimensional electrostatics problem. We are solving for the electric field in the presence of a background distribution of dipole moments described by  $\mathbf{J}^{\mathbf{a}}(x)$ . According to the Helmholtz decomposition theorem, any sufficiently smooth vector field on a 2D domain can be written as

$$\mathbf{J}(x) = \mathbf{J}_{\text{curl-free}}(x) + \mathbf{J}_{\text{div-free}}(x) + \mathbf{J}_{\text{harm}}^{\mathbf{a}}(x) \quad (\text{D8})$$

where

$$\nabla \times \mathbf{J}_{\text{curl-free}}(x) = 0 \implies \mathbf{J}_{\text{curl-free}}(x) = \nabla \chi \quad (\text{D9})$$

$$\nabla \cdot \mathbf{J}_{\text{div-free}}(x) = 0 \implies \mathbf{J}_{\text{div-free}}(x) = \nabla \times \mathbf{r} \quad (\text{D10})$$

$$\nabla \times \mathbf{J}_{\text{harm}}^{\mathbf{a}} = \nabla \cdot \mathbf{J}_{\text{harm}}^{\mathbf{a}} = 0 \quad (\text{D11})$$

The curl free part is gauge dependent and can always be removed by a redefinition of the field  $\varphi$ . The divergence-free component encodes local frustrations in the bond variables whereas  $\mathbf{J}_{\text{harm}}^{\mathbf{a}}$  describes topological zero-modes. In the QLRO (spin-wave) phase vortices are energetically suppressed, so  $\nabla \varphi$  is curl-free. As a result, it cannot compensate or screen the divergence-free part of  $\mathbf{J}^{\mathbf{a}}$ , and any such frustration necessarily contributes an increased energy cost. Along the Nishimori line, frustrated configurations are suppressed and bulk disorder merely renormalizes the spin stiffness  $\kappa$ . This is akin to the polarization field renormalizing the dielectric constant of the medium.

The only part of  $\mathbf{J}$  that remains relevant in the spin-wave description is the harmonic mode  $\mathbf{J}_{\text{harm}}^{\mathbf{a}}$ , which captures the dependence of the free energy on the topological sector  $\mathbf{a}$ . In particular, we may write

$$\mathbf{J}_{\text{harm}}^{\mathbf{a}} = \frac{\sum_i a_i \hat{e}_i}{L} \quad (\text{D12})$$

where  $\hat{e}_i$  denotes the unit vector in the  $i$ th direction and  $a_i$  are now shifted to the symmetric integer range  $\{-\lfloor N/2 \rfloor, \dots, \lfloor N/2 \rfloor\}$ . The presence of such a harmonic mode increases the energy of the configuration. Assuming that the spin-wave field  $\varphi$  is itself periodic on the cylinder, we find that the additional energy cost is simply given by

$$\frac{\kappa}{2} |c_{\mathbf{a}}|^2 \int_0^L d^2x \frac{1}{L^2} = \frac{\kappa}{2} |\mathbf{a}|^2 \quad (\text{D13})$$

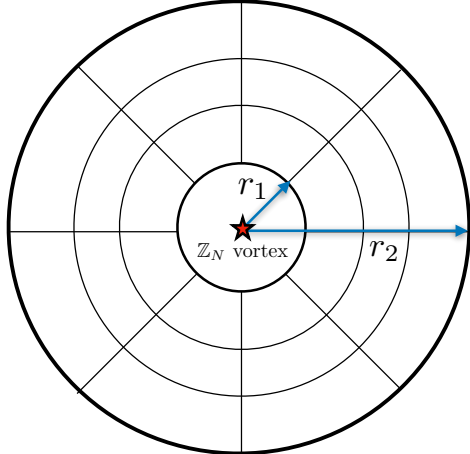


FIG. 7. **Partition function on annulus.** In the QLRO phase, local frustrations remain unimportant but topological modes become important since their energy no longer scales with system size  $L$ . On the annulus, these modes arise due to non-trivial homology. Different winding number sectors around the annulus can be interpreted as a placing different  $\mathbb{Z}_N$  vortex charges in the hole.

which is independent of system size. Thus, we conclude that in the QLRO phase, the winding number probabilities become system size independent due to these topological modes.

$$P(\mathbf{a}|\mathbf{e}) \sim e^{-\frac{\kappa}{2}|\mathbf{a}|^2} \quad (D14)$$

This results in a fractional value for the coherent information, implying a fractionally decodable phase.

## 2. CMI

We now consider the CMI given by the following combination of entropies

$$\begin{aligned} I(A : C|B) = & - \sum_{\mathbf{e}_{AB}} \mathcal{Z}[\mathbf{e}_{AB}] \log \mathcal{Z}[\mathbf{e}_{AB}] \\ & - \sum_{\mathbf{e}_{BC}, E_A} \mathcal{Z}[\mathbf{e}_{BC}, E_A] \log \mathcal{Z}[\mathbf{e}_{BC}, E_A] \\ & + \sum_{\mathbf{e}_B, E_A} \mathcal{Z}[\mathbf{e}_B, E_A] \log \mathcal{Z}[\mathbf{e}_B, E_A] \\ & + \sum_{\mathbf{e}_{ABC}} \mathcal{Z}[\mathbf{e}_{ABC}] \log \mathcal{Z}[\mathbf{e}_{ABC}] \quad (D15) \end{aligned}$$

These are entropies of frustration. In both the ordered and disordered phases, we know the CMI must be exponentially decaying. We now provide a qualitative argument for why the CMI is expected to saturate in the QLRO phase, implying  $\xi_M = \infty$ , based on a Gaussian spin wave ansatz.

Recall that crucially within the Gaussian spin wave approximation, bulk disorder is irrelevant and simply renormalizes the stiffness  $\kappa$ . This is just as in the ordered phase where frustrations are exponentially suppressed. Thus the first and last terms effectively don't contribute in Eq. (D15). The important distinction however between the ordered and QLRO phase is the emergence of the topological zero modes whose energy no longer scales with system size and are thus not energetically suppressed in the  $L \rightarrow \infty$  limit. These modes appear on an annulus due to non-trivial homology. The anyon charges  $E_A$  appearing in the  $BC$  and  $B$  contributions in Eq. (D15) can be viewed as  $\mathbb{Z}_N$  vortices placed on the holes of the annulus Fig. 7. The corresponding zero modes they source takes the form

$$\mathbf{J}_{\text{harm}}^{\mathbf{a}}(r) = \frac{E_A \hat{e}_\theta}{r} \quad (D16)$$

where  $\hat{e}_\theta$  denotes the angular unit vector and  $E$  is again shifted to the symmetric integer range  $\{-[N/2], \dots, [N/2]\}$ . Consequently, the partition function for an annulus with inner and outer radii given by  $r_1$  and  $r_2$  respectively and with vortex charge  $E$  in the hole scales as

$$\mathcal{Z}[E] \sim \left[ \frac{r_1}{r_2} \right]^{\pi \kappa E^2} \quad (D17)$$

Now consider annuli  $B$  and  $BC$  in Eq. (D15). Since  $B$  has inner and outer radii given by  $r_A$  and  $r_B$  whereas  $BC$  has inner and outer radii given by  $r_A$  and  $r_C$ , we find that

$$\begin{aligned} \mathcal{Z}[\mathbf{e}_B, E_A] & \sim \left[ \frac{r_A}{r_B} \right]^{\pi \kappa E_A^2} \\ \mathcal{Z}[\mathbf{e}_{BC}, E_A] & \sim \left[ \frac{r_A}{r_C} \right]^{\pi \kappa E_A^2} \quad (D18) \end{aligned}$$

If we scale these radii proportionately,  $r_{A,B,C} \rightarrow \lambda r_{A,B,C}$ , the zero-mode contributions to the partition function remain unchanged. This scale invariance directly implies that the conditional mutual information saturates to a finite, nonzero value, and consequently that the associated Markov length diverges. We therefore conclude that the QLRO phase must be an information critical phase.